

# Trace element geochemical evolution and groundwater origin in North Rukuru–Songwe alluvial aquifer of northern Malawi

Harold Wilson Tumwitike Mapoma<sup>1,2</sup> · Xianjun Xie<sup>1</sup> · Yapeng Zhu<sup>1</sup> ·  
Yaqing Liu<sup>1</sup> · Gertrude Cynthia Sitolo-Banda<sup>2</sup>

Received: 12 December 2015 / Accepted: 28 April 2016 / Published online: 11 May 2016  
© Springer-Verlag Berlin Heidelberg 2016

**Abstract** This study used multivariate analysis and geochemical modeling to appreciate the trace element evolution in North Rukuru–Songwe alluvial aquifer of northern Malawi. From the isotopic studies, the  $\delta^2\text{H}/\delta^{18}\text{O}$  ratios revealed that groundwater is of meteoric origin through vertical recharge and mixing processes. The isotopic depletion along the west–east transect is due to mixing and fractionation processes. Generally, the *d*-excess value approximated the *y*-intercept of global meteoric water line of 10, which ruled out the influence of secondary evaporative processes on isotopic variation. Hierarchical cluster analysis identified four distinct clusters (C1, C2, C3 and C4) in the study area. Among these four clusters, it was observed that C1 had relatively high median concentrations of Fe (716.7  $\mu\text{g/L}$ ), Cr (0.85  $\mu\text{g/L}$ ), Pb (7.90  $\mu\text{g/L}$ ) and Sb (3.80  $\mu\text{g/L}$ ), while C2 was characterized by high levels of Cu (3.20  $\mu\text{g/L}$ ). Cluster 3 was comparably defined by high median levels of F (1.00 mg/L) and Mn (338  $\mu\text{g/L}$ ), while C4 revealed high median concentrations of As (8.70  $\mu\text{g/L}$ ), Ba (635  $\mu\text{g/L}$ ), Li (22.2  $\mu\text{g/L}$ ), Ni (2.80  $\mu\text{g/L}$ ), Se (6.20  $\mu\text{g/L}$ ) and Sr (677  $\mu\text{g/L}$ ). Clusters C1 and C4 described a flow path along the North Rukuru River, which is characterized by higher levels of evaporites as shown by higher concentrations of Na, K, Cl and  $\text{SO}_4$ . It was also

observed that this path was defined by high levels of  $\text{HCO}_3$  and total hardness. The principal component analysis suggests that carbonate dissolution and silicate weathering are the main mineralization control mechanisms. Furthermore, it is revealed that samples in the west had higher factor scores for As, Ba, Li, Ni, Se and Sr (with higher TDS), while the eastern is characteristic of higher heavy metals (Fe and Pb). Geochemical modeling using PHREEQC showed that surface complexation reactions significantly impact trace elements of higher redox state. In addition, inverse modeling confirms the significance of carbonate dissolution, silicate weathering and cation exchange processes along the North Rukuru River flow path.

**Keywords** Geochemical modeling · Alluvial aquifer · Trace elements · Groundwater · Multivariate statistics · Stable isotopes · Karonga

## Introduction

Groundwater is a convenient source of water for domestic and irrigation use in rural areas of Malawi. Its assumed higher quality relative to surface water makes it a perfect resource. However, the reliance on groundwater has its own disadvantages. Contaminated groundwater is hazardous to the public who rely heavily on this resource. For instance, anthropogenic activities such as agricultural practices and industrial development can mobilize and elevate contaminants in groundwater (Valipour 2014a).

Groundwater chemical composition is controlled by various factors of which mineral dissolution, evapotranspiration and anthropogenic activities or amalgamation of these processes is primary (Fass et al. 2007; Ghabayen

✉ Harold Wilson Tumwitike Mapoma  
hmapoma@poly.ac.mw

✉ Xianjun Xie  
xjxie@cug.edu.cn

<sup>1</sup> School of Environmental Studies and State Key Laboratory of Biogeology and Environmental Geology, China University of Geosciences, Wuhan 430074, China

<sup>2</sup> Department of Physics and Biochemical Sciences, University of Malawi, The Polytechnic, P/Bag 303, Blantyre 3, Malawi

et al. 2006; Mapoma et al. 2014). Water, being an excellent chemical reaction medium and solution, promotes geochemical activities such as surface complexation reactions that control the chemistry of groundwater. The dissolution and reactions of chemical elements in groundwater are promoted by inherent factors such as redox conditions, pH variations, optimal temperature and respiration. Thus, mobilization and immobilization of potentially toxic elements from geogenic materials depend on redox processes and pH besides physical factors (Smedley and Kinniburgh 2002). Also, redox processes control the degradation and preservation of anthropogenic contaminants. Some dissolved elements are more prevalent under reducing conditions while others prefer oxidizing conditions. It is a fact that potency of a hazardous element depends on chemical reactions and speciation. Readily soluble elements are potentially hazardous than immobile species. After all, the potency of an element to human health depends on its characteristics, concentration, exposure duration, exposure route, bio-concentration and bioaccumulation potential. Most significant contaminants that have drawn enough attention in recent years are trace elements found in groundwater. Groundwater has a wider range of chemical composition where complex processes and human activities control the distribution of trace elements in groundwater (Chen et al. 2007).

There is a paucity of information on trace elements and no published records on stable isotopes so far in Karonga district. The lack of information on trace elements is one reason that prompted this study. Karonga's economy is agro based and relies on cash crops such as cotton and rice. Rice is an excellent accumulator of trace elements such as arsenic (Bhattacharya et al. 2012); however, rice plays an important role in the world agriculture (Valipour 2015c; Valipour et al. 2015). If considerable amounts of trace elements exist in groundwater, they may be transferred up the food chain and affect human health depending on amount consumed and exposure route and duration.

Coupled to trace element analysis, stable isotope studies are very important in understanding the groundwater hydrochemistry. Stable oxygen and hydrogen isotopes have proven very useful in groundwater studies (Fontes et al. 1980; Gat and Tzur 1968; Mapoma et al. 2014, 2016; Subyani 2004). Site-specific stable isotope ratios can be compared to the stable isotope values of precipitation that have not been evaporated having a linear relationship of  $\delta^2\text{H} = 8\delta^{18}\text{O} + 10$  ( $R^2 = 0.95$ ) (Craig 1961). Also, a local meteoric water line (LMWL) can be constructed from isotopic data obtained from local sites. Most LMWLs have slopes of  $8 \pm 0.5$ , but a range of 5–9 can be expected (USGS 2004). Processes such as evaporation or mixing with evaporated water can cause the data to plot below the meteoric water line along lines that intersect the MWL at

the location of the original un-evaporated composition of the water. Factors that control the isotopic character of precipitation at a given location are the temperature of condensation, temperature of precipitation and the degree of rainout of the air mass (USGS 2004).

According to USGS (2004), the distribution of isotopic compositions on a regional scale is controlled by (1) altitude effect where the  $\delta^{18}\text{O}$  and  $\delta^2\text{H}$  values of precipitation decrease with increasing altitude on windward side, (2) latitude effect where the  $\delta^{18}\text{O}$  and  $\delta^2\text{H}$  values decrease with increasing latitude because of the increasing degree of "rainout," (3) continental effect of which the ratios decrease inland from the coast and (4) amount effect in which the greater the amount of rainfall, the lower the  $\delta^{18}\text{O}$  and  $\delta^2\text{H}$  values of the rainfall. However, at a given location the seasonal variation and the weighted average isotopic composition remain fairly constant over a long period of time due to constant climatic conditions from year to year. In regions that experience both summer and winter rainfall, they may observe isotopically heavier precipitation in summer than winter caused by seasonal temperature differences and seasonal changes in moisture sources and storm tracks (USGS 2004).

Shallow groundwater  $\delta^{18}\text{O}$  and  $\delta^2\text{H}$  values reflect the local average precipitation values but are modified to some extent by selective recharge and fractionation processes that may alter the  $\delta^{18}\text{O}$  and  $\delta^2\text{H}$  values of the precipitation before the water reaches the saturated zone (Gat and Tzur 1968). Some of these processes include: evaporation of rain during infiltration, selective recharge, interception of precipitation by the tree canopy and exchange of infiltrating water with atmospheric vapor (USGS 2004).

In small catchments, temporal and spatial variability in ground water and base flow  $\delta$  values may reflect seasonal variability in precipitation  $\delta$  values. However, these variations are less extreme and usually delayed, relative to the temporal variations that occur in precipitation (Turner et al. 1987).

In this study, we first deduced the provenance of groundwater using stable hydrogen and oxygen isotope fingerprint on groundwater samples taken from community boreholes. Then, the impact of evapotranspiration and irrigation return flows on groundwater chemistry was assessed. Thereafter, the spatial variations of trace elements in groundwater of this area were evaluated using hierarchical cluster analysis (HCA) and principal component analysis (PCA) to profile the possible patterns and causes of the variations. Furthermore, surface complexation reactions of the identified clustered data were modeled using PHREEQC. Following this, inverse modeling of the evolution of groundwater along the North Rukuru flow path was carried out to observe the changes in groundwater chemistry using median cluster values. This is the first time

that data on stable isotopes and geochemical modeling on trace elements in North Rukuru–Songwe alluvial aquifer of northern Malawi are mutually analyzed and presented.

As stated earlier, we did not find any published records on trace element studies in Karonga, except on Fe and F. And, none of the studies cited in this paper reported on stable isotopes and definitely none so far examined the changes occurring along a flow path using either geochemical modeling or statistical analyses. Otherwise, all cited papers in this study concentrated on groundwater quality conformance with WHO standards. This study therefore aimed at narrowing the gap of knowledge on evolution of groundwater quality in the area. The specific objectives were to (1) evaluate the distribution of groundwater hydrochemistry through cluster analysis, (2) elucidate the possible mineralization control on trace element geochemistry, and (3) examine the evolution of groundwater quality along a flow path using inverse geochemical modeling. The results of this study are anticipated to bridge the information gap needed in addressing groundwater quality and understanding of the causes, fate and implication of trace elements found in this aquifer. Such information acts as a reference point when implementing sustainable groundwater management strategies and policies at local, regional and beyond.

## Study area

The location of the North Rukuru–Songwe aquifer within Karonga district is indicated in Fig. 1. The figure illustrates the sampling sites physical location. The entire district covers an area of 3355 km<sup>2</sup> with a total population of 194,572. Karonga district has a subtropical climate characterized by rainy season (November to May) and dry season (June to October). The average temperature of the district is  $24.4 \pm 5.2$  °C with a maximum annual rainfall of 799 mm (<http://www.karonga.climateemps.com/>). The town of Karonga (Fig. 1) is the center of local and international trade (mostly with Tanzania). It is located within latitudes  $-9.9972^\circ$  to  $-9.9108^\circ$  and between longitudes  $33.8868^\circ$  and  $33.9372^\circ$ . The average elevation of the town is 478 m above mean sea level (amsl).

The geology of Karonga is defined by the Ubendian belt grouping (Chitipa–Karonga) that comprises of several mafic–ultramafic bodies. The flat plain in the north and rolling plain in the southern part with mountains in the east defines the districts topography whose bounding features are distinct of the East African Rift System (EARS). The western margin is bounded by the Nyika Plateau that rises from the rift valley (around 500 m) to 2500 m amsl. In the eastern margin, the surface elevation of the lake is around 500 m amsl (Wright et al. 2014). This flat plain

characteristic feature of the area and the high water holding capacity of soil is ideal for rice growing. However, such soil characteristics and the flat plain topography have negative effect on drainage. Poor drainage results in increased surface soil salinity, while waterlogging accumulates evaporites whose seasonal flushing would consequently affect groundwater quality (Valipour 2014a, b, 2015a, b).

The geomorphology of the area consists of Karoo sediments, Cretaceous–Pleistocene Sediments and Quaternary formations overlying the crystalline Basement complex of Precambrian to lower Paleozoic age (Fagereng 2013; Macheyeke et al. 2015). This Basement complex is distinguished by low-grade metamorphic gneisses (Mafingi Group) belonging to amphibole facies (Chilton and Smith-Carington 1984; Dill et al. 2005). The Karoo sediments consist of conglomerates, sandstones, argillaceous schists and coal seams at the bottom while at the top, arkosic sandstones, marls, and argillaceous schists are apparent (Fagereng 2013; Macheyeke et al. 2015). The sediments have low porosity because they are well bonded by calcite and hardened. Karoo occurs to the north of the area in the west of Karonga and again in the south of the district. They are excellent sources of coal: Nkana and Livingstonia coalfields are prominent examples (Wright et al. 2014).

Cretaceous–Pleistocene sediments are found in small narrow elongated patches, running parallel to the shores of the lake where crumbly sandstones, unconsolidated sands, sandy marls, clays and conglomerates of desert origin are defining features. The permeability and porosity of these rocks are probably high.

Quaternary formations consistent of lacustrine deposits (alluviums, colluviums, lacustral deposits) are well developed in the immediate vicinity of the lakeshore. The strata contain clays, silts, sands and gravels and are intersected in many cases, with a predominance of fine elements and wide variations of facies (Wright et al. 2014). The thickness of the alluvial sediments is very variable along Lake Malawi but tends to increase closer to the shore to a maximum of 60 m. The aquifers formed of fluvial and lacustral sediments are heterogeneous both vertically and horizontally (Wright et al. 2014).

The sampled groundwater is from alluvial aquifers that furnish better yield (Mapoma and Xie 2014; Mapoma et al. 2014). The exact study area within the district (Fig. 1) is dissected by rivers North Rukuru, Kibwe, Rufira, Kyungu and bounded by Songwe (north end of study area). General groundwater flow is from the western highlands toward the lake in the east. The recharge is mostly high rainfall in the hills that contributes to lateral in-flow with infiltrating rainfall contributions while the Lake Malawi acting as a sink. The aquifer in the region is probably semi-confined.

Geothermal activities are observed in some parts of the district. Notable geothermal areas are those located in

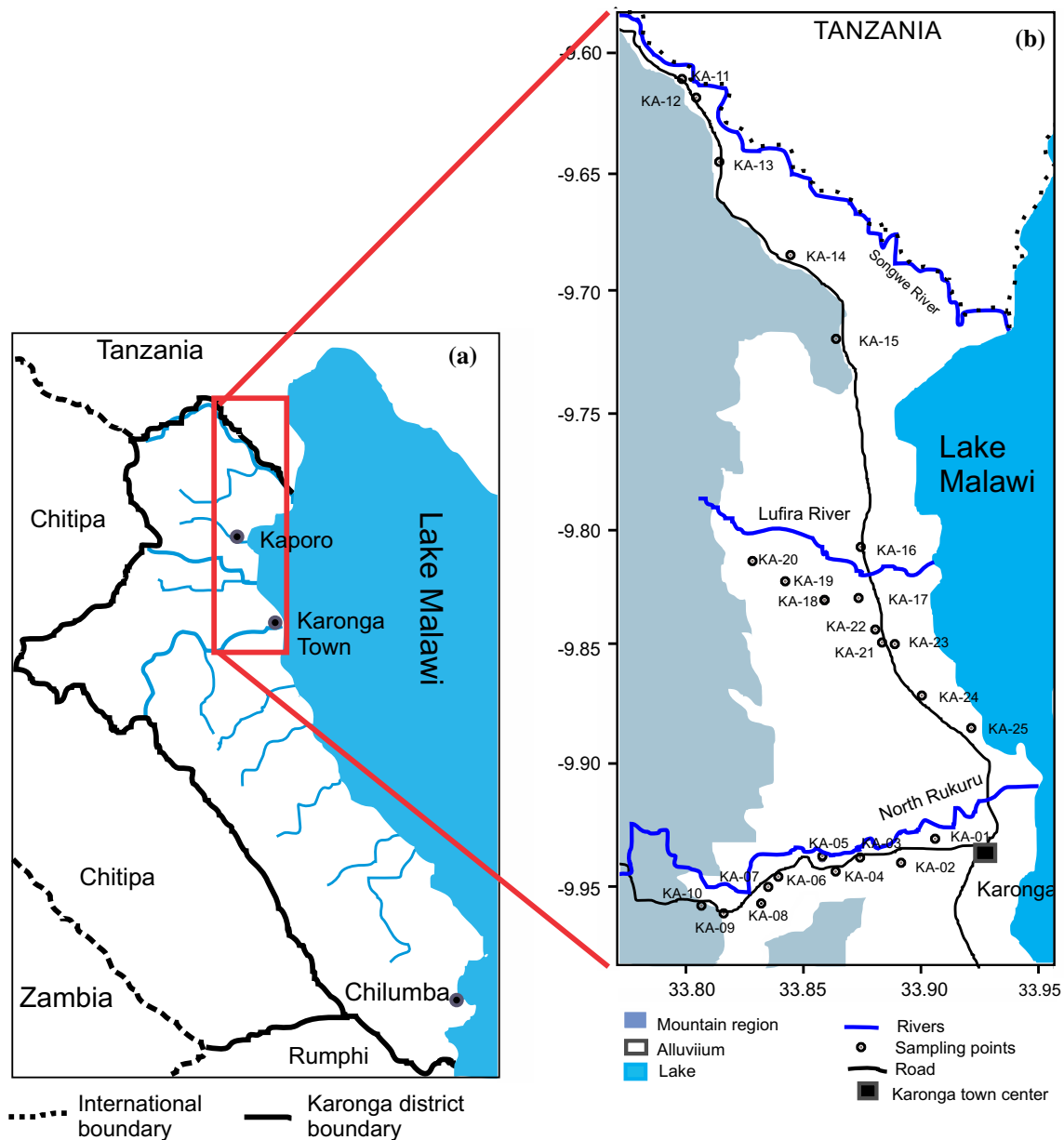


**Fig. 1** Approximate district of Karonga **a** showing the administrative boundaries with Chitipa district, Rumphi (south) and international boundary with Tanzania (north). The study area **b** extruded from

**a** showing the sampling points, geographic features and hydrological setting. The eastern margin (mountain) in **b** is characteristic of basement complex and Karoo (with significant pockets of coal)

Mpata Gap through which North Rukuru passes on its way from the Nyika Mountain Ranges (Dulanya et al. 2010; Fagereng 2013).

## Materials and methods

### Sampling and sample analysis

A total of 25 samples from communal boreholes were drawn in Karonga during the month of April 2015. The

borehole depth records in the area show a range between 35 and 60 m. The 0.45- $\mu\text{m}$  membrane filters were used to strain the samples while filling up the sampling bottles. Twenty-five samples for cation analyses were stored in 50-ml polypropylene bottles and acidified to  $\text{pH} \leq 2$  using  $\text{HNO}_3$ . A duplicate set of 25 samples for anion analysis was not acidified. Thereafter, the temperature-controlled samples were transported and immediately stored in a refrigerator at the Department of Physics and Biochemical Sciences of University of Malawi, The Polytechnic. While in the field, measurements of pH, temperature, electric

conductivity (EC), total dissolved solids (TDS), total hardness and turbidity using standard commercial meters were taken. Alkalinity was analyzed in the Department of Physics and Biochemical Sciences' chemistry laboratory following the prescribed APHA titration technique. Site elevation and coordinates were measured using a portable handheld global positioning system (GPS).

Thereafter, major and trace element constituents were analyzed by inductively coupled plasma optical emission spectrometry (ICP-OES) at State Key Laboratory of Biogeology and Environmental Geology of China University of Geosciences (Wuhan) within 1 week of sampling. The average analytical error for major and trace chemical constituents using ICP-OES is less than  $\pm 5\%$ . Also, anions chloride (Cl), sulfate (SO<sub>4</sub>), fluorides (F) and nitrate (NO<sub>3</sub>) were determined by ion chromatography (IC) (Dionex ICS 1100) with a detection limit of 0.01 mg/L. The observed ionic balance error was within  $\pm 5\%$ .

The  $\delta^{18}\text{O}$  and  $\delta^2\text{H}$  values were measured using a Finnigan MAT 253 stable isotope ratio mass spectrometer at the State Key Laboratory of Biogeology and Environmental Geology, China University of Geosciences in Wuhan.  $\delta^{18}\text{O}$  values were determined through equilibration with H<sub>2</sub>O–CO<sub>2</sub> at 25 °C for 24 h followed by continuous introduction to the mass spectrometer using a Thermo Finnigan GasBench online gas preparation system.  $\delta^2\text{H}$  was measured by reaction with Cr at 850 °C, using an automated Finnigan MAT H/Device (Thermo Scientific). The  $\delta^{18}\text{O}$  and  $\delta^2\text{H}$  values were measured relative to internal standards calibrated using Vienna Standard Mean Ocean Water (V-SMOW). Isotopic composition ( $\delta^{18}\text{O}$  and  $\delta^2\text{H}$ ) was reported in standard  $\delta$  notation representing per mil deviations from the V-SMOW standard (Eq. 1), where

$$\delta^2\text{H}(\text{or } \delta^{18}\text{O}) = \frac{R_{\text{sample}} - R_{\text{standard}}}{R_{\text{standard}}} \times 1000 \quad (1)$$

$$\text{with } R = \frac{{}^2\text{H}}{{}^1\text{H}} \text{ or } \frac{{}^{18}\text{O}}{{}^{16}\text{O}}$$

Precisions for  $\delta^2\text{H}$  and  $\delta^{18}\text{O}$  were  $\pm 1.0$  and  $\pm 0.1\%$ , respectively. Deuterium excess values (*d*-excess) were calculated by  $d = \delta^2\text{H} - 8 \times \delta^{18}\text{O}$  in order to evaluate the changes in moisture sources.

### Data analysis and interpretation

All statistical analyses were done using IBM SPSS version 22 (International Business Machines Corporation, New York). A one-sample Student's *t* test was done to compare the *d*-excess computation data with the GMWL *y*-intercept value. This was done to observe the significance of secondary evaporative processes on isotopic signature. The number of samples together with their respective chemical

and physical parameters (Table 1) made the study a multivariate problem. In this study, HCA and PCA were applied to the dataset. The objective of HCA was to examine and classify groundwater samples based on distribution of the hydrochemical dataset. The Euclidian distance was used as a similarity/dissimilarity measure, whereas the Ward's linkage method was used to link clusters. PCA was used to identify underlying variables that explain the pattern of correlations within the observed physicochemical elements. The aim was to identify a small number of factors that essentially explain most of the variance observed in variables. Mostly, the PCA tried to explain the relationship between redox (and pH) and the studied trace elements.

Prior to multivariate analysis, the variables with below detection limit values  $>25\%$  and additive variables (TDS and EC) were excluded in the analysis (Cloutier et al. 2008; Levins and Gosk 2008). Stable oxygen and hydrogen isotopes were excluded as well. In some samples, it was determined that SO<sub>4</sub> was below detection limit (bdl). In this case, the value of SO<sub>4</sub> for such samples was replaced with the detection limit value of ICP-MS. Furthermore, skewness of data, Shapiro–Wilks test of normality, ANOVA and MANOVA were used as explained in “Results and discussion.”

Geochemical modeling was achieved through PHREEQC version 3 (Parkhurst and Appelo 1999) with the Minteq v4 (Allison et al. 1991) as the main database. The model was run to provide speciation results, saturation indices, surface complexation reactions and inverse modeling on the groups of data identified in multivariate's HCA.

## Results and discussion

### Groundwater chemistry and trace element variations

Table 1 presents the results of in situ measurements and laboratory results. In terms of physical properties, pH variations are apparent among sampling points. The pH observed in Table 1 was slightly acidic to neutral (6.0–7.1). The mean pH indicates that the groundwater is mainly of slightly acidic nature consistent with studies elsewhere in Malawi (Mapoma and Xie 2014; Mapoma et al. 2014; Mkandawire 2004; Wanda et al. 2011, 2013). From previous studies, silicate mineral weathering and carbonate dissolution are viable processes controlling the variations in water quality of Karonga (Wanda et al. 2013).

As indicated in Table 1, the laboratory analysis included a wide spectrum of trace elements found in groundwater. Most of these elements come from natural sources and are mobilized by inherent groundwater conditions, water





activity, microbial respiration and human-induced stabilization. The drawdown of the groundwater level due to pumping, dissolution and exsolution of gases ( $\text{CO}_2$  and  $\text{O}_2$ ), mixing of  $\text{O}_2$ -rich water with relatively deeper anoxic water due to drawdown and recovery of groundwater levels during wet season are all activities that can destabilize the groundwater equilibrium (both physical and chemical) state. Waterlogging in rice-growing season (Valipour 2014a) and probable hard pan formation that enhance flood holding capacity of the surface soil may induce anoxic conditions in the groundwater by limiting  $\text{O}_2$  transport from/exchange with the atmosphere. Thus, the  $\text{O}_2$  available within the confinement of the aquifer may be depleted during aerobic respiration/decomposition of organic matter by microorganisms. Such processes may simultaneously alter pH, temperature and Eh, consequently affecting dissolution/precipitation, ion exchange, surface complexation and sorption processes.

In this study, beryllium (Be) and mercury (Hg) were not detected in all samples. Few samples (<50 %) showed some levels of cobalt (Co) and zinc (Zn), while  $\approx 60$  % had vanadium (V), cadmium (Cd), boron (B) and aluminum (Al) present (Table 1). Comparing with drinking water standards, a few exceptions were identified to be above threshold. From Table 1, it can be extracted that Mn (23 % of samples), As (20 %) and Fe (24 %) violated the threshold values of 400, 10 and 1500  $\mu\text{g/L}$ , respectively (WHO 2011). Only one sample (KA-05) showed fluoride higher than 1.5 mg/L limit value for drinking water.

Areas along the North Rukuru River (Fig. 1) have relatively higher turbidity with KA-10 showing highest TH (Table 1). Similarly,  $\text{HCO}_3^-$  values >250 mg/L (WHO 2011) (except KA-01) were observed along the North Rukuru area with KA-09 presenting the highest concentration compared to the rest of the study area. It was also observed that the North Rukuru area was relatively enriched in Na, Cl,  $\text{SO}_4$  and F. KA-09 had the highest Na content in the sample. This suggests that the area is more prone to evaporitic concentration effect and probably enrichment from surface contamination due to fertilizer application (organic and inorganic). In terms of trace elements, similar general observation as that of major elements was made for As, B, Ba and Sr. The highest concentration of As, B, Ba, Li and Sr was observed for KA-09. These elements are consistent with coal activities, which were evident in this area, especially around KA-09 and KA-10. KA-09 had very low concentration of Mn and Fe. Higher concentration of Mn was observed for KA-03, KA-04, KA-11, KA-15, KA-16, KA-18, KA-19 and KA-21 with the highest value obtained for KA-16. Lower values of Fe were observed along the North Rukuru River. The highest value of Fe in this study was observed for KA-25 followed by KA-18, KA-13 and KA-12, respectively. The

same samples had relatively high levels of Pb which co-occurs with Fe and probably affected by industrial activities such as transportation along the busy main road between Karonga town and Malawi–Tanzania border. Mechanisms responsible for these variations are identified in section “Multivariate statistical analysis.”

### Stable isotopes of oxygen and hydrogen

In the study area, stable isotope investigation of groundwater is a new field. Investigation of isotopes coupled with geochemical analysis adds value and more information on the structure of the aquifer, especially the groundwater origin. The stable isotope data can offer insight into the regional studies that try to distinguish between shallow and deep aquifers (Praamsma et al. 2009) and identify zones of interaction and recharge processes (Horst et al. 2007; Subyani 2004; Sukhija et al. 2006). Thus, they are excellent tracers for determining the origin of groundwater. Since  $\delta^{18}\text{O}$  and  $\delta^2\text{H}$  are influenced by processes affecting the water rather than the solutes, they can identify waters that have undergone evaporation, recharge under different climatic conditions than the present, and mixing of waters from different sources.

The stable isotopes analyzed in this study and their statistical summaries are presented in Table 1. Positive values of  $\delta^{18}\text{O}$  and  $\delta^2\text{H}$  indicate enrichment when compared to SMOW (Talabi 2013) contrary to our observations. The regression analysis of oxygen and hydrogen isotopes is illustrated in Fig. 2. The figure includes the global meteoric water line (GMWL) defined by the average relationship between hydrogen and oxygen isotope ratios in natural terrestrial waters (Craig 1961). Normally, the  $\delta^2\text{H}$

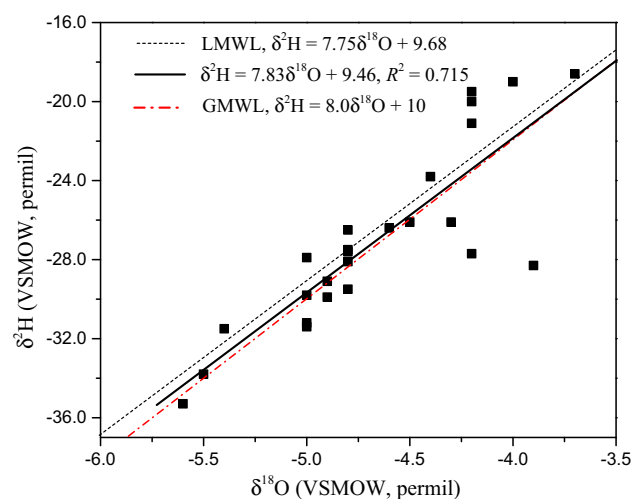


**Fig. 2** The  $\delta^2\text{H}$  versus  $\delta^{18}\text{O}$  plot of groundwater samples from Karonga north compared to GMWL (Craig 1961) and LMWL (Monjerezi et al. 2011)



and  $\delta^{18}\text{O}$  diagram is useful in interpreting information on the origin of groundwater. Included in the figure is the generalized LMWL (Mapoma et al. 2014; Monjerezi et al. 2011). The LMWL runs slightly parallel to the GMWL (Fig. 2).

About 64 % of the groundwater samples plotted on or close to the GMWL and LMWL, producing a regression line defined by  $\delta^2\text{H} = 7.83\delta^{18}\text{O} + 9.46$  with a regression coefficient ( $R^2$ ) of 0.715 that suggests a meteoric origin with a mean isotopic composition as indicated in Table 1 (Boutaleb et al. 2000; Mapoma et al. 2014; Monjerezi et al. 2011). Therefore, the alignment of isotopic composition close to the GMWL and LMWL demonstrates a precipitation origin of groundwater in the studied area. Compared to studies done elsewhere in Malawi (Mapoma et al. 2014; Monjerezi et al. 2011), the isotopic composition in this study was relatively enriched. This may be attributed to differences in rainout (amount effect), local conditions, altitude effect and latitudinal differences (Mapoma et al. 2014; Monjerezi et al. 2011). Samples whose isotopic composition shifted apart from the GMWL and LMWL and plotted to the right suggest the effect of processes such as evaporation within the unsaturated zone during recharge or mixing with an evaporated source. Elevated temperature may cause an increase in  $\delta^{18}\text{O}$  but not  $\delta^2\text{H}$  of water while increasing  $\delta^{18}\text{O}$  of rocks as water attempts to reach isotopic equilibrium. This is mostly observed in geothermal exchange. In this study, such geothermal activities were not investigated. But the shift in isotopic composition to the left may be attributed to temperature variations. Delayed infiltration, low hydraulic conductivity and base flow recharge may be the cause of discernible differences in isotopic composition unlike in fractured basement where infiltration is high with little modification of isotopic ratio (Mapoma et al. 2014).

As shown in the literature, evaporation and exchange with rock minerals are common fractionation processes that affect the relationship between  $\delta^2\text{H}$  and  $\delta^{18}\text{O}$  (Fontes et al. 1980). Hence, the shifting apart indicates the action of combined local processes such as selective infiltration, a certain degree of direct percolation that do not change the isotopic composition of the original rainwater, some degree of fractionation in the vadose zone and most probably surface water contribution (several rivers present) and mixing mechanisms by anthropogenic activities, especially groundwater drawing.

The process of evapotranspiration increases the concentration of dissolved salts in water. A plot of  $\delta^{18}\text{O}$  versus TDS is used in this study to extricate the relationship between evaporation and dissolution of evaporites (Fig. 3a). In this figure, there is no general relationship between TDS and variation in isotopic composition. However, a decrease in  $\delta^{18}\text{O}$  is observed for TDS

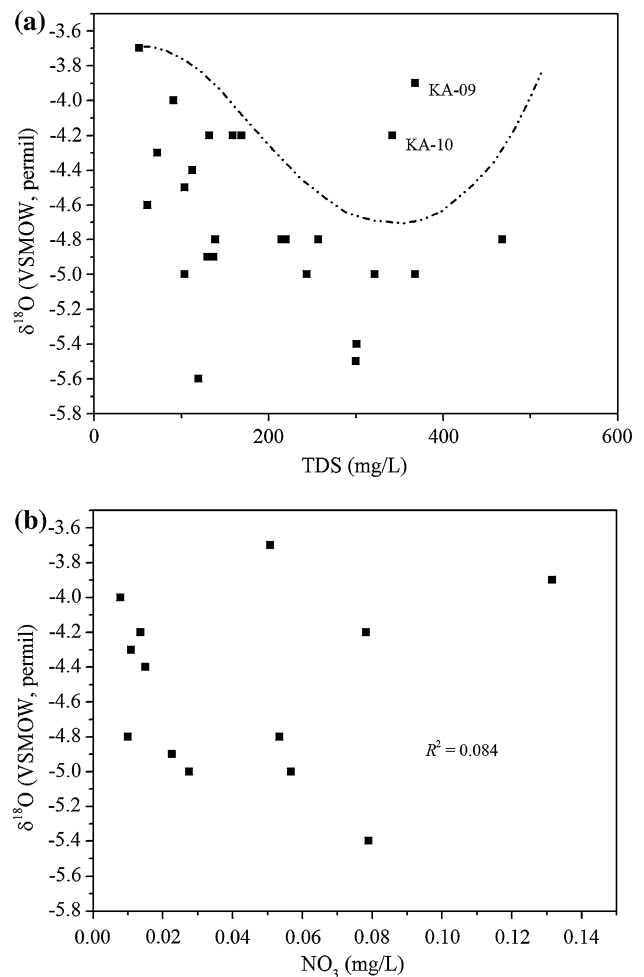


**Fig. 3** Relationship between  $\delta^{18}\text{O}$  with TDS (a) and  $\text{NO}_3$  (b) used to explain the impact of evapotranspiration and irrigation return flows, respectively. Difference between KA-09 and KA-10 is discussed in this section “Stable isotopes of oxygen and hydrogen”

$\leq 350$  mg/L suggesting minimal effect of evaporation during recharge. But, the observation for  $\text{TDS} \geq 350$  mg/L may be due, in part, to evaporative effect, especially for the two samples KA-09 and KA-10. Therefore, the general observation is that the isotopic variation may arise from mixing of groundwater along the flow paths.

It is noted from Table 1 that KA-09 and KA-10 differ in hydrochemistry although sited at almost the same elevation along the North Rukuru River. Probably, local conditions in the aquifer matrix and variations in sediment mineralogy could explain these differences. Most of the ionic concentration values for KA-09 are more than twice that of KA-10. Further investigation in sediment geochemistry is needed. Visually, KA-09 surface soils are fine darkish gray silt with a coal-like look while those of KA-10 were observed to be sandy soils (high vertical recharge). Furthermore, KA-09 (relative to KA-10) seems to be highly impacted by agriculture activities such as fertilizer

application in cotton fields, animal husbandry, closeness to the road and evaporitic enrichment as observed by the high concentrations of Na, Cl,  $\text{HCO}_3$ ,  $\text{SO}_4$ , F,  $\text{NO}_3$ , As, B, Ba, Li and Sr. KA-10 represents a groundwater that is characterized by high total hardness in this area (Table 1). It may also be reasonable to assume that local flow paths (from mountain to river) define the differences between these two paths since KA-09 seems to be located on a longer local flow path from mountain front than KA-10, hence more enriched.

Irrigation return flow may modify  $\delta^{18}\text{O}$  as water infiltrates and percolates. Using Fig. 3b, it was possible to investigate the effect of irrigation practices on groundwater hydrochemistry. Even so, the relationship between  $\delta^{18}\text{O}$  and  $\text{NO}_3$  was very poor to support the impact of irrigation return flow (Fig. 3b) probably due to high water holding capacity of soils and formation of hard pan in rice-growing season. The non-equilibrium conditions during source water evaporation are conveniently assessed using the  $d$ -excess values (Table 1). The  $d$ -excess is dependent on relative humidity and sea surface temperature in the moisture source region (Breitenbach et al. 2010). But temperature has a rather weak influence on stable isotopes from precipitation in tropical regions (Aggarwal et al. 2004). Yet, stable isotopes are controlled by amount of precipitation and the degree of air mass rainout during moisture transport (USGS 2004). Moreover, the  $d$ -excess of the continental atmospheric vapor mass may be altered by contribution from secondary evaporative processes (Marfia et al. 2004). In this study, a one-time sampling of groundwater and analysis of isotopes was done, which preclude the analysis of  $\delta^{18}\text{O}$  versus precipitation. A statistical analysis using one-sample  $t$  test shows that the  $d$ -excess values approximate the  $y$ -intercept of the GMWL of 10 (Fig. 4). As such the influence of secondary evaporative processes is irrelevant (Marfia et al. 2004). However, KA-09 and KA-10 have a  $d$ -excess that is significantly lower than 10 (i.e.,  $\leq 5.8$ ) indicating effect of local conditions on isotopic variation.

## Multivariate statistical analysis

### Hierarchical cluster analysis

The sufficiently large number of variables makes this study a multivariate problem as mentioned in “Materials and methods.” The HCA outcome from a standardized (Cloutier et al. 2008; Levins and Gosk 2008) dataset performed on the 25 samples is a dendrogram (Fig. 5). The phenon line drawn at a linkage distance of 9.5 produced four stable and geochemically distinct clusters (C1, C2, C3 and C4). Although these clusters are distinct, the dendrogram reveals some levels of similarities between the clusters.

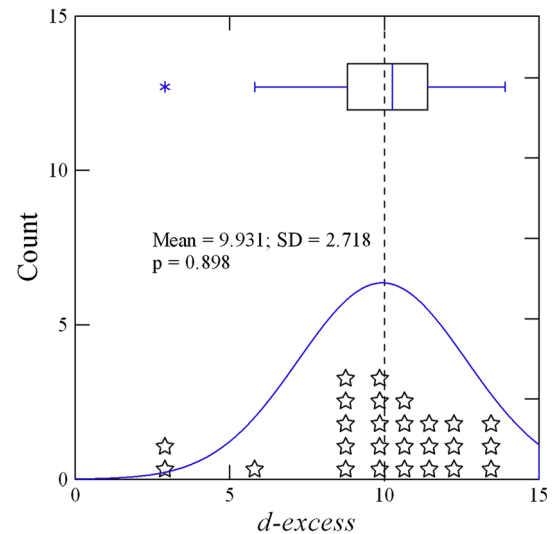


**Fig. 4** One-sample  $t$  test result comparing computed  $d$ -excess values with the  $y$ -intercept of the GMWL

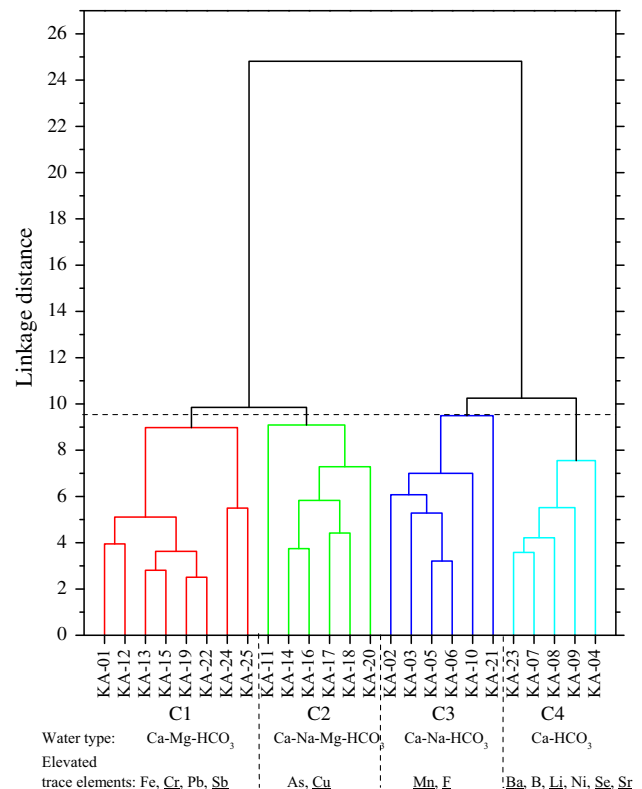


**Fig. 5** Dendrogram for the groundwater samples illustrating the demarcation of clusters with profiling variables (water types and trace elements) shown for each of the seven clusters

Samples clustered in C1 and C2 are linked at a lower distance. Similar observation is made for clusters C3 and C4. But, C1 and C2 samples are linked to C3 and C4 samples at an elevated distance showing some levels of dissimilarities between the two sets of pairs. Thus, the

expected results are that the general geochemistry of these clusters evolves from one cluster to another between pairs and that marked differences are expected when comparing the cluster pair of C1/C2 to that of C3/C4.

To assess the validity of clusters obtained, a MANOVA model was estimated using TDS, EC and  $\delta^2\text{H}$  as validity criterion variables while cluster membership was the independent variable. From the variables left out for being stable or additive, these three criterion variables were selected because they were found to significantly correlate with each other ( $p < 0.001$ ) unlike  $\delta^{18}\text{O}$ , Eh and temperature ( $p > 0.05$ ). The overall MANOVA model was significant ( $F = 70.9, p < 0.001$ ), supporting the idea that these variables can be predicted by knowing to which cluster they belong. The individual univariate statistics were also significant ( $p < 0.001$ ) further supporting this finding. In Table 2, the median concentration of relatively elevated minor and trace elements is shown and depicted on the dendrogram (Fig. 5) as part of the profiling variables.

Generally, on a set of additional variables  $\text{NO}_3$ , Al, Cd, V, Zn and ANOVA test for significant differences, the clusters show distinct differences (Table 2) except for temperature and  $\delta^{18}\text{O}$ . It is also observed from the same table that variations among clusters were apparently insignificant in the cases of K, Si, As, Fe, Mn, Ni and Pb. As such, the cluster profile in terms of minor and trace elements is better explained by the marked differences in Ba, Cr, Cu, F, Li, Sb, Se and Sr (underlined in Fig. 5). As mentioned in previous paragraph, the highest concentration of these profiling trace elements is indicated in bold, while the lowest is underlined in association with the cluster (Table 2). It is also noted that C2 has groundwater that is relatively more oxidized while C4 is more reduced of the four clusters observed (Table 2). Furthermore, relatively hard water is envisaged for C4, while lowest total hardness is observed in C2. According to Table 2, C2 represents relatively hard waters, while C3 describes samples consistent with a set of higher dissolved salts that describe salinity levels (Na, Cl,  $\text{SO}_4$  and Mg). Higher TDS is apparent in C4 while lowest for C2.

From the Schoeller diagram, the median water types were deduced for each cluster (Fig. 6). These general water types for the individual clusters are presented in the dendrogram as additional profiling variables. All four clusters displayed a bicarbonate-dominated water type similar to previous studies in the area (Wanda et al. 2013). Based on water types deduced for each cluster, the befitting and clear evolution of groundwater can be traced along a flow path that follows the west–east transect beneath the North Rukuru River (C4, C3 and C1). The groundwater evolves from the Ca– $\text{HCO}_3$  through the mixed Ca–Na– $\text{HCO}_3$  to Ca–Mg– $\text{HCO}_3$  type. Thus, the more hard water evolves into water with higher salinity descriptors along the flow

path prior to discharge into Lake Malawi. As such, evaporite levels are expected to be heightened away from the recharge zone compared to carbonates as seen in the C4–C3 pair of clusters. It is also noted that total hardness follows this trend (Table 2) supplementing to this observation. In fact, TDS profile shows that toward the lake the groundwater has low dissolved solids. Groundwater close to the recharge zone (West) contains higher concentrations of major elements than in the east, while the converse is true for trace elements due to various inherent geochemical mechanisms including redox conditions, precipitation, evapotranspiration and pH-dependent dissolution. Also, dilution effect occurs as the aquifer thickness increases closer to the shore compared to the western zone (see section describing the study area). The low TDS observed for C2 is due to short flow paths. Organic matter may also play a key role in the amount of  $\text{HCO}_3$  realized from decomposition. The redox-sensitive elements As and Fe display an inverse evolution profile from each other (As:  $\text{C4} > \text{C3} > \text{C1}$ ; Fe:  $\text{C1} > \text{C3} > \text{C4}$ ). Thus, the mechanisms involved in elevating these two elements may be incongruent dissolution processes. While arsenic levels may vary according to changes in redox and pH conditions (such as reductive dissolution and pH dependent), iron content may arise from hydrolysis/dissolution of Fe-carbonates and ferromagnesian minerals, consistent with amphibole facies. As groundwater evolves from the Ca– $\text{HCO}_3$  to ultimately Ca–Mg– $\text{HCO}_3$ , As increases while Fe decreases probably through precipitation and involvement in sorption processes. The trends observed for the flow path along the North Rukuru River can also be described on a latitudinal differences, C2–C1–C3. However, this may not follow a proper groundwater flow path even though remarkable observations may be discerned. Due to absence of sediment lithology in the study area, it was not feasible to prove the impact of sediment geochemistry on trace elements. However, inverse modeling was performed on the C4–C3 flow path and discussed later on for potential mineral transfers inferred from the general lithology of the alluvial aquifer of Malawi. In general, C4 and C1 show a remarkable profile consistent with higher levels of trace elements and that boron levels are in the order  $\text{C4} > \text{C3} > \text{C1}$  along the North Rukuru River (Table 2). These are the areas where intensive rice farming, irrigation, high evapotranspiration and industrial activities are more pronounced while the western part is dominated by animal raising, maize growing and cotton.

Further studies on the relationship between trace elements using HCA (figure not shown) yielded the lowest linkage distances for Ba, Sr and Li. This implies that these elements and their concentrations profiles are affected by similar geochemical processes. Similar low linkages were observed for Cr, Pb and Fe.

**Table 2** Median values of geochemical and physical characteristics of each cluster identified using HCA

Parameter	C1	C2	C3	C4	ANOVA	
					F	Sig.
Class members	8	6	6	5		
Eh (mV)	-5.45	<b>14.50</b>	-8.75	<b>-21.70</b>	6.74	0.002
pH	6.51	<u>6.31</u>	6.57	6.73	4.03	0.021
TH (mg/L)	122	<u>54</u>	236	<b>298</b>	27.38	0.000
Calcium	33.0	<u>14.0</u>	76.6	<b>97.8</b>	24.73	0.000
Mg (mg/L)	9.4	<u>4.8</u>	<b>16.6</b>	10.8	5.44	0.006
Na (mg/L)	12.7	<u>11.6</u>	<b>55.9</b>	38.7	6.74	0.002
K (mg/L)	<u>2.10</u>	2.20	3.45	<b>5.00</b>	2.43	0.093
HCO <sub>3</sub> (mg/L)	182	<u>94</u>	385	<b>494</b>	41.48	0.000
Cl (mg/L)	<u>3.30</u>	4.65	<b>8.45</b>	7.30	3.86	0.024
SO <sub>4</sub> (mg/L)	<u>0.76</u>	1.60	<b>9.40</b>	2.00	5.49	0.006
F (mg/L)	0.50	<u>0.30</u>	<b>1.00</b>	0.80	4.52	0.013
Si (mg/L)	22.8	24.8	24.7	24.1	0.86	0.475
As (µg/L)	<u>5.90</u>	8.85	8.30	8.70	1.91	0.158
Fe (µg/L)	<b>716.7</b>	112.3	13.8	<u>2.2</u>	2.38	0.099
Mn (µg/L)	328	299	<b>338</b>	<u>171</u>	1.06	0.388
Ba (µg/L)	157	<u>107</u>	285	<b>635</b>	6.36	0.003
Cr (µg/L)	<b>0.85</b>	0.35	<u>0.30</u>	0.60	5.12	0.008
Cu (µg/L)	<u>0.55</u>	<b>3.20</b>	0.75	0.80	3.54	0.032
Li (µg/L)	1.65	<u>1.30</u>	4.40	<b>22.20</b>	4.64	0.012
Ni (µg/L)	2.05	2.60	<u>1.95</u>	<b>2.80</b>	1.25	0.315
Pb (µg/L)	<b>7.90</b>	5.65	<u>5.30</u>	6.00	2.72	0.071
Sb (µg/L)	<b>3.80</b>	2.30	<u>1.80</u>	3.50	4.37	0.015
Se (µg/L)	3.65	<u>3.55</u>	3.90	<b>6.20</b>	5.07	0.009
Sr (µg/L)	178	<u>100</u>	324	<b>677</b>	16.82	0.000
Stable or additive variables						
EC (µS/cm)	279	<u>165</u>	563	<b>679</b>	32.28	0.000
TDS (mg/L)	138	<u>82</u>	272	<b>342</b>	19.18	0.000
Temperature (°C)	28.9	28.6	29.40	29.20	2.21	0.117
δ <sup>2</sup> H	-26.3	<b>-25.0</b>	<u>-29.9</u>	-28.3	3.96	0.022
δ <sup>18</sup> O	-4.7	<b>-4.4</b>	<u>-5.0</u>	-4.9	2.81	0.065
Missing >25 % data						
Turbidity (NTU)	0.37 (0.63)	<b>1.85 (0.83)</b>	1.81 (0.50)	0.03 (0.20)		
NO <sub>3</sub> (mg/L)	0.7 (0.25)	0.8 (0.67)	3.15 (0.33)	<b>3.5 (1.00)</b>		
Al (µg/L)	<b>5.3 (0.63)</b>	1.7 (0.67)	1.6 (0.50)	2.1 (0.40)		
B (µg/L)	3.95 (0.29)	1.25 (0.33)	3.15 (1.00)	<b>17.2 (1.00)</b>		
Cd (µg/L)	<b>0.2 (0.88)</b>	0.1 (0.83)	0.1 (0.33)	0.1 (0.20)		
Co (µg/L)	0.5 (0.50)	<b>0.7 (0.17)</b>	0.2 (0.17)	bdl		
V (µg/L)	0.25 (0.38)	2.5 (0.50)	1.2 (0.67)	<b>11.0 (0.80)</b>		
Zn (µg/L)	0.5 (0.13)	4.4 (0.5)	<b>19.7 (0.17)</b>	1.5 (0.20)		

Bracketed values fraction of samples whose values were detected among the total cluster members. Bold italics represents positive and negative median value indicates highest relatively oxidizing condition and highest relatively reducing condition, respectively. Bold values highest median value. Underlined lowest median value. Italics variations among the groups' median values were not significant at 95 % confidence level

bdl below detection limit

Even though stable isotopes (δ<sup>2</sup>H and δ<sup>18</sup>O) were not included in the HCA study, the median values accrued to each cluster follows an enrichment profile of the order

C2 > C1 > C4 > C3 (Table 2). According to Fig. 7 in relation to observed median values of stable isotopes for the clusters (Table 2), it shows that groundwater in the

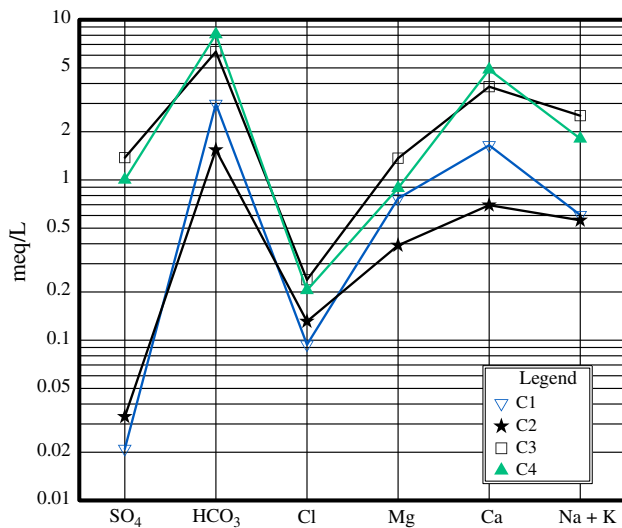


**Fig. 6** Schoeller diagram used to deduce the most dominant ion in the system and provide insight into the median groundwater type

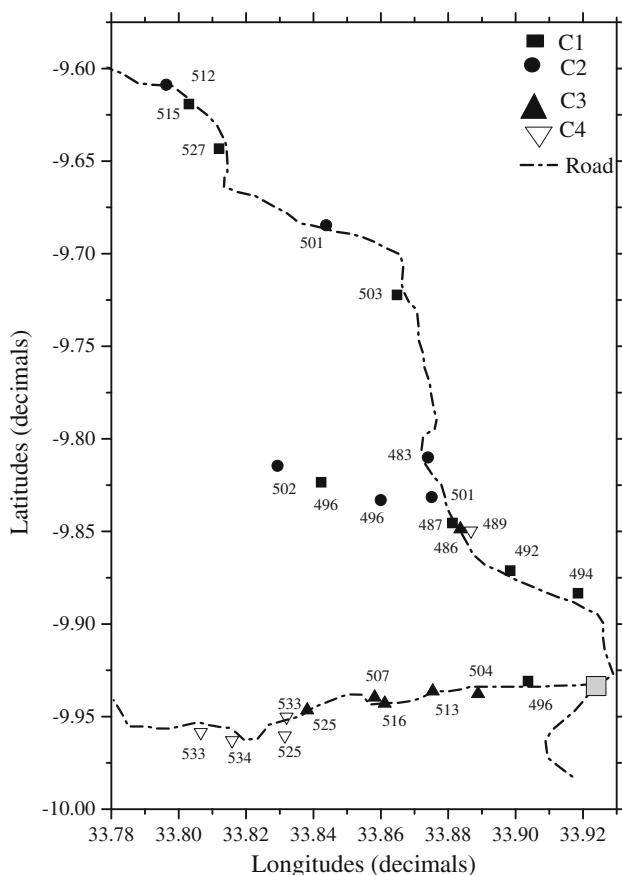


**Fig. 7** Location of clusters (and their members) together with the specific site elevation (meters above mean sea level) used to visualize when explaining the trends in trace elements and isotopes evolving from west to east of the study area

south of the area is more depleted than in the northern part (clearly as  $C2 > C1 > C4$ ). Similarly, the altitude variations along the longitudes (Fig. 7) are illustrated by the  $C4 > C3$  profile. Therefore, the variation in isotopic signature might be attributed to various factors such as rock–water interaction, selective recharge, fractionation process including evapotranspiration, canopy interception of precipitation and exchange of infiltrating water with atmospheric vapor (USGS 2004).

The distinct clusters underscore the fact that hydrogeological conditions along the flow path affect the chemistry of the groundwater as is the impact of redox conditions and pH changes. Anthropogenic activities contribute to the variations in minor and trace element loadings. The water type shows that Mg–Na ion exchange is plausible along the flow path and is included in the inverse modeling later on in this paper.

*Principal component analysis*

A complete dataset is necessary to effectively use multivariate statistics’ PCA. All variables were positively skewed and majority had significant skewness (Table 1). The failure of most variables in the Shapiro–Wilks normality test ( $p < 0.05$ ) and the skewness prompted the log transformation of the variables prior to invoking PCA. Based on eigenvalues, the PCA provided information on the participation of the individual chemical parameters in several influence factors. The PCA retained six components based on the Kaiser Normalization criterion for which only the components with eigenvalues greater than 1 are significant. The six independent factors rotated using varimax normalization explained 78.31 % of the total variance. The communalities ( $>0.5$ ) extracted for each variable using principal component met the acceptable levels of explanation of the variables in factor analysis results.

Each of the components satisfied the criteria where maximizing the variance implies maximizing the range of the loadings that tend to produce either extreme (positive or negative) or near-zero loadings. Each component is characterized by a few high loadings (highlighted in bold) and many near-zero loadings which fulfills the objective of the rotation (Cloutier et al. 2008). The first three components explain 56.29 % of the total variance (Table 3). Thus, they account for the majority of the variance in the dataset. The low loading of component 6 shows its insignificance in the explanation of the factors having one high loading of Si which in itself is a stable variable across the samples studied.

Component 1 explains the greatest amount of the variance (34.25 %) and is characterized by high positive loadings in Ca, TH, Ba, Li, Se and Sr with mild loadings of

**Table 3** Varimax rotated principal component matrix showing the six significant principal components based on eigenvalue  $\geq 1$ 

	PC1	PC2	PC3	PC4	PC5	PC6
Eh	-0.262	<b>-0.822</b>	-0.084	-0.044	-0.027	0.348
pH	0.216	<b>0.817</b>	0.076	0.036	-0.016	-0.162
As	0.047	<u>0.628</u>	-0.051	-0.315	-0.176	-0.078
Ca	<b>0.790</b>	0.167	0.270	-0.170	-0.022	-0.341
Cl	0.236	-0.006	<b>0.889</b>	-0.131	-0.080	0.100
F	0.041	<u>0.595</u>	<u>0.519</u>	-0.108	0.093	0.033
Fe	-0.240	-0.133	-0.103	<b>0.830</b>	0.159	0.041
HCO <sub>3</sub>	<u>0.682</u>	<u>0.513</u>	0.411	-0.020	-0.007	-0.255
K	0.076	<u>0.699</u>	0.038	-0.334	0.045	0.153
Mg	0.236	0.214	<b>0.813</b>	0.177	0.007	-0.230
Mn	<u>-0.579</u>	0.239	0.113	0.002	0.288	-0.001
Na	0.372	<u>0.642</u>	<u>0.521</u>	0.043	0.004	0.011
SO <sub>4</sub>	0.069	0.098	<b>0.882</b>	-0.103	-0.146	0.096
Si	0.096	-0.228	0.084	-0.089	-0.037	<b>0.789</b>
TH	<b>0.732</b>	0.200	0.453	-0.094	-0.017	-0.351
Ba	<b>0.849</b>	0.147	0.041	-0.043	-0.059	0.250
Cr	-0.060	-0.084	-0.011	0.394	<b>0.805</b>	0.032
Cu	-0.342	0.118	-0.216	-0.469	0.273	0.340
Li	<b>0.724</b>	0.371	-0.055	-0.072	0.023	0.348
Ni	0.306	0.252	-0.450	0.349	<u>-0.573</u>	0.064
Pb	-0.045	-0.149	-0.079	<b>0.924</b>	-0.006	-0.101
Sb	0.172	0.085	-0.373	-0.122	<b>0.774</b>	-0.045
Se	<b>0.768</b>	0.113	0.332	-0.028	0.321	0.059
Sr	<b>0.822</b>	0.454	0.154	-0.002	0.023	-0.028
Total eigenvalue	8.220	2.666	2.622	2.228	1.907	1.151
Explained variance (%)	34.25	11.11	10.93	9.28	7.95	4.80
Cumulative % variance	34.25	45.36	56.29	65.57	73.51	78.31

*Bold values* loadings  $>0.7$ , *underlined values* significant mild loadings

HCO<sub>3</sub> and Mn (Table 3). This component can be interpreted as a factor of carbonate dissolution (especially calcite) and hardness profile. Thus, it describes the Ca-HCO<sub>3</sub> water type envisaged in the cluster analysis. It may also explain the influence of CO<sub>2</sub> on the elevated HCO<sub>3</sub> in the system either from atmospheric dissolution or microbial degradation of organic matter. This factor is more apparent for C4. Areas in the C4 may be influenced by high loads of organic matter from animal waste (grazing lands) and autochthonous litter which may be biodegraded by microorganisms and hence elevating HCO<sub>3</sub>. It is observed that the highest factor scores for this component are for samples KA-09, 10 and 11 which are very close to the recharge zone. The mild loading of Mn signifies its importance in influencing dissolution of minerals and participation in complexation as Mn-hydroxides/oxide. Complexation is one of the control mechanisms of trace element loads in groundwater such as Ba, Li, Se and Sr (Merkel et al. 2005). The direct relationship between Mn and Eh is noted from this component. Mn is a redox-sensitive element and can be involved in alteration of redox

conditions in the system. Formation of Mn complexes and the alteration of redox conditions may mobilize other trace elements in the groundwater.

Component 2 explains the significance of pH and Eh on the mineralization of minor and trace elements in the system. This is because of the influence of pH and Eh on As and F. It has been observed and document that As increases with increasing pH (and decreasing Eh) values (Smedley and Kinniburgh 2002). This is clear from the analysis as the Eh value shows a high negative loading relative to As and F. This component shows that the main process for the observed As and F may be reductive dissolution and pH-dependent dissolution of As-containing and F-containing minerals. The higher factor scores for this component are for areas along North Rukuru and Lufira rivers that are consistent with reducing conditions and high pH.

The abundance of As in sediments is not yet known in the study area as such the low concentrations observed compared to As laden areas around the world may be attributed to various processes such as co-precipitation/dissolution, redox conditions, pH, microbial activities and

probably dissolution of As-containing minerals. The factor explains further that an increase in Na is concomitant with increased levels of HCO<sub>3</sub> loadings. This may suggest that Na levels are influenced by changes in pH as HCO<sub>3</sub> levels affect pH.

Component 3 explains the sulfate and chloride elevation in the system from evaporite dissolution of minerals such as mirabilite and halite. The significant mild loading of F in this component suggests the dissolution of F-containing minerals. However, the low concentration of F observed in this study and the low loading of Ca in this component signify that the dissolution of fluorite (CaF<sub>2</sub>) is not the main control. Micaceous minerals, such as biotite (K(Mg,Fe)<sub>3</sub>(AlSi<sub>3</sub>O<sub>10</sub>)(F,OH)<sub>2</sub>), may contribute to the levels of F through rock–water interaction. Similar to component 2, the highest factor scores for this component fall along the North Rukuru River, and they cluster mostly to the eastern part where aquifer thickness is higher to promote disintegration–dissociation and dissolution processes. Also, in the eastern part, there is intensive development, industrial and agriculture-related activities. These activities may contribute to levels of F relative to those in the western part.

Figure 8a provides a summary on the position of the loadings of chemical parameters in the rotated plane defined by the axes of components 1 and 2, while Fig. 8b illustrates the position of the parameters with respect to components 1 and 3. From the positions of the parameters

in space, a conceptual descriptive term is defined for each of the components based on their characteristic loadings (Fig. 8a, b). Because of the association of Ca, HCO<sub>3</sub> and TH, component 1 is a characteristic of hardness and carbonate dissolution. Component 2 is defined by the high positive loading of pH and high negative loading of Eh, which may be defined as Eh–pH factor. The association of Mg, SO<sub>4</sub> and Cl loadings defines the evaporite dissolution for component 3. From the two figures, halite dissolution is insignificant as shown by the distance in positions of the loadings of Na and Cl.

The highest factor scores for component 4 show elevated levels of Fe and Pb in the areas close to the main road (KA-11, KA-12 and KA-25). Heightened levels of Fe may be due to rock–water interaction along the flow path as groundwater ages. Vehicular emissions along the busy main road between Karonga and Tanzania (Figs. 1, 7) might have contributed to relatively elevated levels of Pb besides geogenic sources in the past when vehicles used leaded petrol. Such emissions onto the surface would find its way into groundwater through infiltrating rain water. Besides, the growing industrial activity in the study area is another contributing factor. The negative loading of sulfate relative to Fe shows minimal impact of oxidation of Fe-sulfide mineral in elevated Fe concentrations. It may suggest that the geogenic source of Fe is from dissolution of Fe-carbonate minerals such as siderite and probably ferromagnesian minerals.

Component 5 shows high loadings of Sb and Cr with mild loadings of Ni. The factor scores for this component show that such high loadings occur for samples taken very close to the roads (KA-05, 06, 11, 12, 15, 16, 21, 22 and 25). The location of these sampling points is synonymous with coal use and mining activities. Coal contains a myriad of trace metals of which Sb, Cr and Ni are part.

Component 6 is difficult to explain because it has only Si with high positive loading. This factor may explain silicate weathering of pure silicates and aluminosilicates. The levels of silicate in the entire study area have little variations, and the ANOVA test shows insignificant variations (Table 2). As such, it is not possible to attribute this factor to a specific cluster and process, but to the geochemical process that may persist in the entire area (especially silicate weathering). The cation exchange and silicate weathering may be incongruent process in the study area as shown by the negative loadings of Ca and Mg and the positive loadings of Na and K in this component.

*Implication of multivariate analysis on trace elements and water quality*

The multivariate analysis suggests that the observed concentrations may be due to processes occurring within the

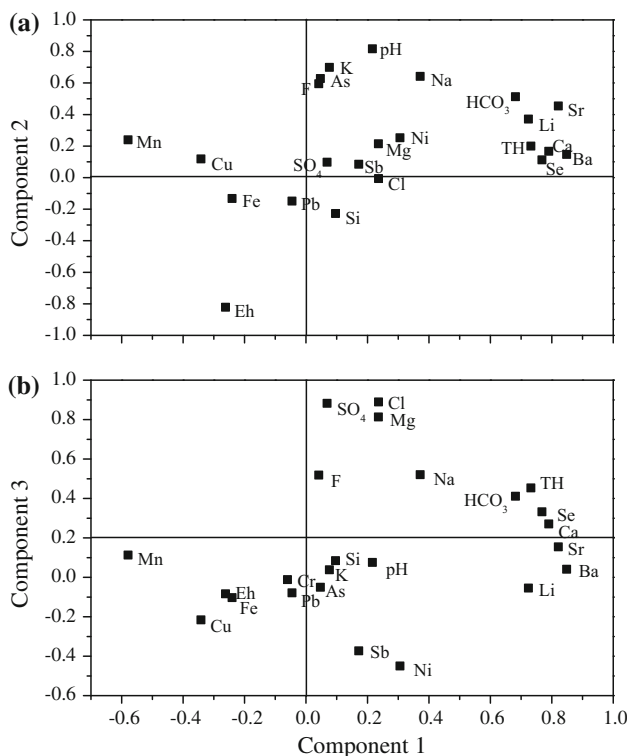


**Fig. 8** Plot of loadings in rotated space of the first two components (a) and that of component 1 versus component 3 (b)

aquifer such as adsorption mechanisms, redox conditions, incongruent dissolution, complexation and presence of limiting mineral phases. Ion exchange may be involved as well as some elements like Al may be readily exchanged by Mg while Li may be displaced by divalent cations from the silicate minerals. Formation of complexes can lead to adsorption of toxic and undesirable elements such as As, Mn and Cd. The form in which the element exists in the groundwater entails the toxic potential of the element. Mobility of ions is influenced by pH and redox state of groundwater. For instance, redox-sensitive trace elements are more mobile under low pH and toxic conditions. For instance, Cd, Cu, Pb and Zn can increase adsorption on oxide hydroxides under elevated pH (Mapoma et al. 2014; Salbu and Steinnes 1995). Others such as Fe and Mn are mobile under low pH and (or) anoxic conditions. In contrast, some oxyanion-forming trace elements, e.g., As, Cr, Se and V, are generally more mobile under high pH conditions.

The Eh values observed indicate reduction of  $\text{NO}_3^-$ , oxidation of organic matter, reduction of  $\text{Fe}^{3+}$  to  $\text{Fe}^{2+}$  (Merkel et al. 2005). The low Eh values may be due to depletion of dissolved oxygen during microbial metabolism. In this case, microbial activities begin to depend on  $\text{O}_2$ /energy from reduction of  $\text{NO}_3^-$ ,  $\text{Fe}^{3+}$  and  $\text{SO}_4^{2-}$ . Such activities contribute to increase in  $\text{HCO}_3^-$ , low  $\text{SO}_4^{2-}$ , pH progression from slightly acidic to neutral and variation in dissolved trace elements. Coal mining and the recent uranium mining activities in the western margin could be other sources of variations of F.

Besides Eh and pH factors, time elapsed since recharge significantly affects chemical evolution of trace elements in groundwater. The elongated contact time between the liquid phase and the aquifer matrix ensures enough time for dissolution, chemical reactions and sorption processes to occur that controls the elemental load of the groundwater. Local mixing of groundwater may affect localized physical–chemical changes. The variation in elevation shows that groundwater flow may also be subject to varying changes in hydraulic conductivity which may affect the geochemistry. Active faulting in the study area has been observed. As recent as 2009, seismic activities are on recorded (Fagereng 2013; Macheyeki et al. 2015), suggesting that the presence of faults may have a remarkable impact on groundwater flow regime and infiltration rate which in turn can affect the chemical variations.

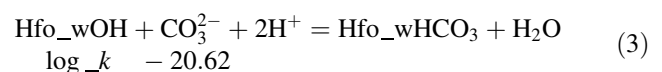
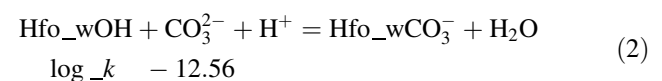
## Geochemical modeling

### *Speciation and surface complexation reactions*

Speciation studies were done using PHREEQC on the median values observed for the four classes of groundwater (Table 4). As mentioned earlier, there were variations in

redox conditions and pH which may explain in part the differences in redox-sensitive elements such as  $\text{SO}_4^{2-}$ , Fe, As, Se, Cr, Sb and Mn. The variations have already been discussed in the preceding chapters, and the causes have been suggested from the multivariate analysis. Species present in the liquid phase interact in various ways such as sorption and ion exchange, precipitation, redox reactions and complexation. Surface complexation is one of the various mechanisms involved in controlling trace element mobilization in groundwater. Differences in redox conditions, pH, the ion chemistry distribution and subsequent competition define the amount of sorbates onto surface complexes. The redox state of redox-sensitive elements shows in which state the species adsorb more to the surface. The prevailing conditions in the aquifer, which facilitates the adsorption of elements to surface complexes, provide a means of abatement of toxic elements.

Complexation reactions significantly influence dissolution/precipitation of minerals and concentration of ions in the liquid phase. In this study, a two-layer surface complexation model was used to demonstrate plausible changes that may occur to available species in the groundwater using universal constants. Sorption on hydrous ferric oxide (Hfo) of various species was simulated assuming the complex has weak (Hfo\_w) and strong (Hfo-s) sites on the oxide surface. The universal constants adopted in the study are moles of binding sites ( $\text{Hfo}_w = 2 \times 10^{-4}$  and  $\text{Hfo}_s = 5 \times 10^{-6}$ ),  $600 \text{ m}^2/\text{g}$  of surface area per mass of surface material and  $0.09 \text{ g}$  as the total mass of the surface complex. Minteq v4 database provided the complexation reaction species with  $\text{CO}_3$  complexation reaction taken from Phreeqc.dat (Eqs. 2, 3).



The simulation outcome shows that in terms of density  $\text{H}^+$ ,  $\text{OH}^-$  and  $\text{Ca}^{2+}$  outcompete trace elements on strong sites followed by Pb, Ba and Ni in that order. Similarly,  $\text{HCO}_3^-$ ,  $\text{CO}_3^{2-}$ ,  $\text{OH}^-$ ,  $\text{Mg}^{2+}$  and  $\text{Ca}^{2+}$  occupy a greater surface area on the weak binding site. Despite the density competition, the removal efficiency of trace elements from the liquid phase onto the surface complex shows that Se(VI), Cr(III), Se(IV), Cr(IV) and Pb are retained more onto amorphous iron surface followed by As(V), Sb(V), Cu(II) and As(III), respectively (Table 4). The Fe(III) is involved in formation of amorphous Fe (Hfo) that is why there is an observed reduction in concentration of Fe(III) species compared to that of Fe(II) (Table 4). Reduction processes are therefore critical to the changes in concentration of elements coupled to surface complexation



**Table 4** PHREEQC modeled initial median species concentration for the four clusters and percent remaining in solution after surface complexation modeling

Parameter	C4		C2		C3		C4	
	C <sub>o</sub>	C/C <sub>o</sub> (%)	C <sub>o</sub>	C/C <sub>o</sub> (%)	C <sub>o</sub>	C/C <sub>o</sub> (%)	C <sub>o</sub>	C/C <sub>o</sub> (%)
B	–	–	–	–	2.92 × 10 <sup>-7</sup>	–	1.59 × 10 <sup>-6</sup>	–
Ba	1.14 × 10 <sup>-6</sup>	98.78	7.79 × 10 <sup>-7</sup>	98.97	2.08 × 10 <sup>-6</sup>	99.28	4.63 × 10 <sup>-6</sup>	99.39
Ca	8.24 × 10 <sup>-4</sup>	99.64	3.49 × 10 <sup>-4</sup>	99.66	1.91 × 10 <sup>-3</sup>	99.79	2.44 × 10 <sup>-3</sup>	99.80
Cl	9.31 × 10 <sup>-5</sup>	–	1.31 × 10 <sup>-4</sup>	–	2.39 × 10 <sup>-4</sup>	–	2.06 × 10 <sup>-4</sup>	–
F	2.63 × 10 <sup>-5</sup>	99.96	1.58 × 10 <sup>-5</sup>	–	5.27 × 10 <sup>-5</sup>	–	4.21 × 10 <sup>-5</sup>	–
K	5.37 × 10 <sup>-5</sup>	–	5.63 × 10 <sup>-5</sup>	–	8.83 × 10 <sup>-5</sup>	–	1.28 × 10 <sup>-4</sup>	–
Li	2.38 × 10 <sup>-7</sup>	–	1.87 × 10 <sup>-7</sup>	–	6.34 × 10 <sup>-7</sup>	–	3.20 × 10 <sup>-6</sup>	–
Mg	3.87 × 10 <sup>-4</sup>	99.97	1.98 × 10 <sup>-4</sup>	–	6.83 × 10 <sup>-4</sup>	99.99	4.45 × 10 <sup>-4</sup>	99.96
Na	5.53 × 10 <sup>-4</sup>	–	5.05 × 10 <sup>-4</sup>	–	2.43 × 10 <sup>-4</sup>	–	1.69 × 10 <sup>-4</sup>	99.94
Ni	3.49 × 10 <sup>-8</sup>	49.97	4.43 × 10 <sup>-8</sup>	50.39	3.32 × 10 <sup>-8</sup>	70.85	4.77 × 10 <sup>-8</sup>	72.77
Pb	3.81 × 10 <sup>-8</sup>	0.02	2.73 × 10 <sup>-8</sup>	0.01	2.56 × 10 <sup>-8</sup>	0.05	2.90 × 10 <sup>-8</sup>	0.08
Sb	3.12 × 10 <sup>-8</sup>	–	1.89 × 10 <sup>-8</sup>	–	1.48 × 10 <sup>-8</sup>	–	2.88 × 10 <sup>-8</sup>	–
Si	3.80 × 10 <sup>-4</sup>	–	4.13 × 10 <sup>-4</sup>	–	4.11 × 10 <sup>-4</sup>	–	4.01 × 10 <sup>-4</sup>	–
Sr	2.03 × 10 <sup>-6</sup>	–	1.14 × 10 <sup>-6</sup>	–	3.70 × 10 <sup>-6</sup>	–	7.73 × 10 <sup>-6</sup>	–
As(III)	7.52 × 10 <sup>-8</sup>	27.18	1.13 × 10 <sup>-7</sup>	23.45	1.04 × 10 <sup>-7</sup>	40.03	1.07 × 10 <sup>-7</sup>	37.71
As(V)	3.53 × 10 <sup>-9</sup>	1.44	5.13 × 10 <sup>-9</sup>	0.33	6.98 × 10 <sup>-9</sup>	5.79	9.06 × 10 <sup>-9</sup>	6.86
Cr(II)	1.82 × 10 <sup>-18</sup>	0.01	7.42 × 10 <sup>-19</sup>	0.01	6.30 × 10 <sup>-19</sup>	0.01	1.06 × 10 <sup>-18</sup>	0.01
Cr(III)	1.64 × 10 <sup>-8</sup>	0.00	6.73 × 10 <sup>-9</sup>	0.00	5.77 × 10 <sup>-9</sup>	0.00	1.16 × 10 <sup>-8</sup>	0.00
Cr(VI)	1.31 × 10 <sup>-36</sup>	–	3.80 × 10 <sup>-37</sup>	–	7.73 × 10 <sup>-37</sup>	–	2.80 × 10 <sup>-36</sup>	–
Cu(I)	8.61 × 10 <sup>-9</sup>	86.77	5.00 × 10 <sup>-8</sup>	88.69	1.17 × 10 <sup>-8</sup>	89.84	1.25 × 10 <sup>-8</sup>	92.23
Cu(II)	4.96 × 10 <sup>-11</sup>	18.07	3.28 × 10 <sup>-10</sup>	9.07	9.68 × 10 <sup>-11</sup>	32.40	1.06 × 10 <sup>-10</sup>	37.19
Fe(II)	1.28 × 10 <sup>-5</sup>	–	2.01 × 10 <sup>-6</sup>	–	2.47 × 10 <sup>-7</sup>	–	3.94 × 10 <sup>-8</sup>	–
Fe(III)	2.59 × 10 <sup>-10</sup>	23.92	3.66 × 10 <sup>-11</sup>	12.39	5.15 × 10 <sup>-12</sup>	38.86	1.03 × 10 <sup>-12</sup>	43.62
Mn(II)	5.97 × 10 <sup>-6</sup>	–	5.44 × 10 <sup>-6</sup>	–	6.16 × 10 <sup>-6</sup>	–	3.12 × 10 <sup>-6</sup>	–
Mn(III)	5.03 × 10 <sup>-31</sup>	19.52	8.97 × 10 <sup>-31</sup>	9.71	5.34 × 10 <sup>-31</sup>	34.54	1.59 × 10 <sup>-31</sup>	38.19
SO <sub>4</sub>	7.91 × 10 <sup>-6</sup>	99.9	1.67 × 10 <sup>-5</sup>	99.64	9.79 × 10 <sup>-5</sup>	99.9	2.08 × 10 <sup>-5</sup>	–
HS <sup>-</sup>	Nil	1.7 × 10 <sup>-24</sup>	Nil	1.6 × 10 <sup>-22</sup>	Nil	1.9 × 10 <sup>-25</sup>	Nil	2.7 × 10 <sup>-26</sup>
Sb(III)	3.11 × 10 <sup>-8</sup>	<b>100.5</b>	1.88 × 10 <sup>-8</sup>	<b>100.6</b>	1.47 × 10 <sup>-8</sup>	<b>100.5</b>	2.86 × 10 <sup>-8</sup>	<b>100.6</b>
Sb(V)	1.58 × 10 <sup>-10</sup>	5.15	1.11 × 10 <sup>-10</sup>	1.36	9.09 × 10 <sup>-11</sup>	14.23	1.96 × 10 <sup>-10</sup>	17.76
Se(-2)	4.62 × 10 <sup>-8</sup>	–	4.50 × 10 <sup>-8</sup>	–	4.94 × 10 <sup>-8</sup>	–	7.86 × 10 <sup>-8</sup>	–
Se(IV)	2.08 × 10 <sup>-14</sup>	0.01	1.34 × 10 <sup>-13</sup>	0.00	2.37 × 10 <sup>-14</sup>	0.24	1.69 × 10 <sup>-14</sup>	0.46
Se(VI)	7.83 × 10 <sup>-31</sup>	0.00	5.27 × 10 <sup>-30</sup>	0.00	1.29 × 10 <sup>-30</sup>	0.03	9.63 × 10 <sup>-31</sup>	0.08

– no observed change

Bold value highlights that the initial concentration of Sb(III) increased by a fraction after surface complexation modeling unlike the observations made for other elements

reactions as shown by the decrease in Sb(V) relative to a 5 % increase in Sb(III), decrease in Fe(III) and conversion of SO<sub>4</sub><sup>2-</sup> to form H<sub>2</sub>S (Table 4) after surface complexation reactions are involved. The production of H<sub>2</sub>S was not observed in initial batch modeling. H<sub>2</sub>S reacts with Fe to form Fe-sulfide minerals which play a part in removal of toxic elements such as As. If such production of Fe-sulfides occurs in this aquifer supported by the fairly reducing conditions, it may be one of the many probable causes of the observed low As concentrations in the aquifer. However, the surface complexation model did not yield any

possible precipitating Fe-sulfide minerals. All sulfide minerals were found to be undersaturated with respect to the liquid phase.

Redox-sensitive Mn forms complexes as well, which may also affect the distribution of other species and redox conditions of the groundwater. Thus, the model shows that concomitant to surface complexation, redox processes affect the distribution of trace elements in the alluvial aquifer. The As(III)/As(V) ratio shows that the more toxic arsenic albeit low in the groundwater can be detrimental to the health of people in the study area, especially along the

North Rukuru River where it is relatively higher than the northern area. Besides, surface complexation model demonstrates the effect on saturation state of groundwater through the change in saturation indices of the potential minerals used further in inverse modeling (Table 5). One notable shift is the change from supersaturation to undersaturation of goethite (Table 5) related to reduction of Fe(III) during formation of Hfo. The observation is inverse to that of siderite. Apart from surface complexation and redox processes, the modeling results show that dissolution of carbonates, sulfates, CO<sub>2</sub>, ferroselite, fluorite, halite, ferromagnesian minerals, silicate weathering and precipitation of oxides/oxyhydroxides are part of the control mechanisms of trace element levels in groundwater in this study (Table 5). Precipitation/equilibrium state of groundwater with respect to pure silicates (e.g., quartz) buffer silicate concentrations.

### *Inverse modeling*

Geochemical inverse modeling was done to shade more light on the evolution changes in groundwater along a selected path (North Rukuru River gradient). As classified in the HCA scheme, the boreholes along this path were grouped into C4 (Ca–HCO<sub>3</sub>) and C3 (Ca–Na–HCO<sub>3</sub>) with distinct water profiles. The groundwater is loosely supposed to end up in the groundwater chemistry described by C1 (Ca–Mg–HCO<sub>3</sub>). Therefore, the model was run to understand the evolution of groundwater with distance since these areas were in the same definite flow path. However, C1 was not included in the model. The selected potential mineral phases expected in the Karonga alluvial aquifer, their reactions and accompanied solubility constants are given in Table 5. All the minerals listed were used in the inverse model. CO<sub>2</sub> was included in the model as a product of respiration, which in turn contributes to HCO<sub>3</sub> concentration. Before embarking on inverse modeling, the charge balance was rechecked to be consistent with modeling uncertainty criteria. The charge balance was within the acceptable range for inverse modeling ( $\pm 5$ ) for the two groups of groundwater samples.

The saturation indices of minerals used in inverse modeling (Table 5) show that carbonates, evaporites and (hydr)oxides are generally undersaturated, which could promote dissolution of Ca, Mg, Na, HCO<sub>3</sub>, Fe, F, SO<sub>4</sub> and Sr in order to attain equilibrium between the aqueous and mineral phase of the system. Magnetite (an oxide mineral) and ferroselite could be controlling the concentration of Fe in the aquifer as shown by their supersaturation state. Judging from the saturation state of quartz (Table 5), it is probable that this mineral equilibrates the SiO<sub>2</sub> that would have otherwise been elevated from dissolution of sepiolite and greenalite. Across the clusters, the saturation indices

did not vary much except for goethite where in C1 it is supersaturated while C2 the water is undersaturated after surface complexation reactions were included in the model. It follows that the groundwater varies from supersaturated state to undersaturated state with respect to goethite across the clusters explaining the variations in Fe content among them.

Based on observed trends and saturation state of groundwater (Table 5), magnetite, quartz, goethite and ferroselite were set to precipitate while the rest of the primary minerals were allowed to dissolve once they reached saturation. Carbon dioxide was allowed to dissolve since it was assumed to be available from microbial oxidation of organic carbon. Cation exchange reactions of Ca<sup>2+</sup> and Mg<sup>2+</sup> for Na<sup>+</sup> on exchange sites were included in the model.

Table 5 includes the two most optimum inverse models, out of a possible 8 realized from modeling, for the selected simulations with phase mole transfers for the minerals and gases. According to the two models, the main process is precipitation of calcite and pure silicate with dissolution of CO<sub>2</sub> and silicates such as sepiolite when groundwater evolves from C4 to C3. Calcite precipitates from solution to reach saturation of the new conditions, while CO<sub>2</sub> dissolves to maintain the HCO<sub>3</sub> concentrations. The relatively low concentration of Ba, Ca and Si in C3 compared to C4 is due to precipitation of barite, calcite and pure silicates, while relatively high concentrations of Mg, Na and SO<sub>4</sub> is due to dissolution of ferromagnesian, halite and sulfate minerals as shown by the mole transfers in Table 5.

It is noted that there were no observed mole transfers in dolomite as dolomite is probably due to the slow reaction of dolomite in the natural liquid phase. Also, there were no notable mole transfers in Fe-oxyhydroxides/oxides but release of Fe<sup>2+</sup> from silicate weathering. Fe(II) oxidizes to Fe(III) which forms Hfo as mentioned earlier and involved in complexation reactions. These reactions reduce As and other trace element species. It is noted that As(III) is removed more in C4 than C3 while As(V) is removed more in C3 than C4 that is why total As is higher in C3 since concentrations are significantly greater than those of As(V) (Table 4). It is given in Table 4 that the oxidized state of trace elements is removed more than their reduced counterparts due to groundwater prevalently being reduced. It means that while groundwater evolves from C4 to C3 the species distribution will be affected by the redox state of the new liquid phase during mole transfer. The model further shows that large quantities of calcite produced during mole transfer from C4 to C3 reduce Ca and HCO<sub>3</sub> concentrations, while increased dissolution of sulfates, halite, silicates, fluorite and ferromagnesian minerals relatively elevate SO<sub>4</sub>, Na, Cl, F, Mg and Fe<sup>2+</sup> which changes the groundwater type to Ca–Na–HCO<sub>3</sub> mentioned in HCA.

**Table 5** Potential mineral reactions (and their solubility constants) used in inverse modeling and their saturation indices both before surface complexation reactions and after surface complexation modeling accompanied by the results of inverse modeling

Mineral	Reaction	Solubility product (log <sub>10</sub> K)						Saturation indices <sup>a</sup>						Inverse modeling <sup>b</sup>		
		C1		C2		C3		C4		Model 1	Model 2					
		Initial	After	Initial	After	Initial	After	Initial	After			Initial	After			
Barite	$\text{BaSO}_4(\text{s}) = \text{Ba}^{2+} + \text{SO}_4^{2-}$	-1.43	-1.44	-1.18	-1.18	-0.24	-0.24	-0.59	-0.59	-3.57 × 10 <sup>-7</sup>	-3.57 × 10 <sup>-7</sup>	-0.59	-0.59	-3.57 × 10 <sup>-7</sup>	-3.57 × 10 <sup>-7</sup>	
Calcite	$\text{CaCO}_3(\text{s}) = \text{Ca}^{2+} + \text{CO}_3^{2-}$	-1.08	-1.04	-1.89	-1.84	-0.41	-0.39	-0.06	-0.03	-1.50 × 10 <sup>1</sup>	-1.50 × 10 <sup>1</sup>	-0.06	-0.03	-1.50 × 10 <sup>1</sup>	-1.50 × 10 <sup>1</sup>	
CO <sub>2</sub> (g)	$\text{CO}_2(\text{g}) + \text{H}_2\text{O}(\text{l}) = 2\text{H}^+ + \text{CO}_3^{2-}$	-1.23	-1.27	-1.31	-1.36	-0.98	-1.01	-1.04	-1.07	1.50 × 10 <sup>1</sup>	1.50 × 10 <sup>1</sup>	-1.04	-1.07	1.50 × 10 <sup>1</sup>	1.50 × 10 <sup>1</sup>	
Dolomite	$\text{CaMg}(\text{CO}_3)_2(\text{s}) = \text{Ca}^{2+} + \text{Mg}^{2+} + 2\text{CO}_3^{2-}$	-2.29	-2.21	-3.84	-3.74	-1.06	-1.02	-0.65	-0.59	-	-	-0.65	-0.59	-	-	
Ferroselite	$\text{FeSe}_2(\text{s}) + 2\text{H}^+ + 2\text{e}^- = 2\text{HSe}^- + \text{Fe}^{2+}$	11.55	10.21	11.06	9.14	9.77	8.9	9.25	8.47	-	-	9.25	8.47	-	-	
Fluorite	$\text{CaF}_2(\text{s}) = \text{Ca}^{2+} + 2\text{F}^-$	-2.00	-2.00	-2.75	-2.75	-1.16	-1.16	-1.25	-1.25	1.53 × 10 <sup>-5</sup>	1.53 × 10 <sup>-5</sup>	-1.25	-1.25	1.53 × 10 <sup>-5</sup>	1.53 × 10 <sup>-5</sup>	
Goethite	$\text{FeOOH}(\text{s}) + 3\text{H}^+ = \text{Fe}^{3+} + 2\text{H}_2\text{O}(\text{l})$	0.491	0.53	<b>0.07</b>	<b>-0.79</b>	-0.53	-0.92	-1.09	-1.43	-	-	-1.09	-1.43	-	-	
Greenalite	$\text{Fe}_3\text{Si}_2\text{O}_5(\text{OH})_4(\text{s}) + 6\text{H}^+ = 3\text{Fe}^{2+} + 2\text{H}_4\text{SiO}_4(\text{aq}) + \text{H}_2\text{O}(\text{l})$	20.81	-3.71	-3.45	-7.13	-6.81	-8.66	-8.51	-10.15	-9.98	7.55 × 10 <sup>-8</sup>	7.55 × 10 <sup>-8</sup>	-10.15	-9.98	7.55 × 10 <sup>-8</sup>	7.55 × 10 <sup>-8</sup>
Gypsum	$\text{CaSO}_4 \cdot 2\text{H}_2\text{O}(\text{s}) = \text{Ca}^{2+} + \text{SO}_4^{2-} + 2\text{H}_2\text{O}(\text{l})$	-4.61	-3.91	-3.86	-3.86	-2.61	-2.61	-3.20	-3.20	-	-	-3.20	-3.20	-	8.73 × 10 <sup>-5</sup>	
Halite	$\text{NaCl}(\text{s}) = \text{Na}^+ + \text{Cl}^-$	1.603	-8.96	-8.84	-8.84	-7.94	-7.94	-8.16	-8.16	1.30 × 10 <sup>-4</sup>	1.30 × 10 <sup>-4</sup>	-8.16	-8.16	1.30 × 10 <sup>-4</sup>	1.30 × 10 <sup>-4</sup>	
Magnesianoferrite	$\text{Fe}_2\text{MgO}_4(\text{s}) + 8\text{H}^+ = \text{Mg}^{2+} + 2\text{Fe}^{3+} + 4\text{H}_2\text{O}(\text{l})$	16.86	-3.83	-4.9	-6.60	-8.21	-6.76	-7.49	-7.78	-8.39	2.35 × 10 <sup>-12</sup>	-7.78	-8.39	2.35 × 10 <sup>-12</sup>	2.35 × 10 <sup>-12</sup>	
Magnetite	$\text{Fe}_3\text{O}_4(\text{s}) + 8\text{H}^+ = 2\text{Fe}^{3+} + \text{Fe}^{2+} + 4\text{H}_2\text{O}(\text{l})$	3.403	7.98	6.9	4.71	3.10	3.04	2.32	1.43	0.81	-	1.43	0.81	-	-	
Mirabilite	$\text{Na}_2\text{SO}_4 \cdot 10\text{H}_2\text{O}(\text{s}) = 2\text{Na}^+ + \text{SO}_4^{2-} + 10\text{H}_2\text{O}(\text{l})$	-1.114	-10.93	-10.93	-10.6	-10.6	-8.69	-8.69	-9.69	8.73 × 10 <sup>-5</sup>	-	-9.69	-9.69	8.73 × 10 <sup>-5</sup>	-	
Quartz	$\text{SiO}_2(\text{s}) + 2\text{H}_2\text{O}(\text{l}) = \text{H}_4\text{SiO}_4(\text{aq})$	-4.00	0.53	0.57	0.57	0.56	0.56	0.56	0.55	-2.26 × 10 <sup>1</sup>	-2.26 × 10 <sup>1</sup>	0.55	0.55	-2.26 × 10 <sup>1</sup>	-2.26 × 10 <sup>1</sup>	
Septiolite	$\text{Mg}_2\text{Si}_3\text{O}_7 \cdot 5\text{OH} \cdot 3\text{H}_2\text{O}(\text{aq}) + 4\text{H}^+ + 0.5\text{H}_2\text{O}(\text{l}) = 2\text{Mg}^{2+} + 3\text{H}_4\text{SiO}_4(\text{l})$	15.76	-6.82	-6.65	-8.04	-7.83	-6.07	-5.98	-5.87	7.52	7.52	-5.87	-5.76	7.52	7.52	
Siderite	$\text{FeCO}_3(\text{s}) = \text{Fe}^{2+} + \text{CO}_3^{2-}$	-10.24	-1.11	-1.07	-2.36	-2.30	-2.53	-2.51	-3.08	-3.05	-	-3.08	-3.05	-	-	
Strontianite	$\text{SrCO}_3(\text{s}) = \text{Sr}^{2+} + \text{CO}_3^{2-}$	-9.27	-2.91	-2.87	-3.60	-3.55	-2.35	-2.33	-1.78	-1.75	1.50 × 10 <sup>1</sup>	1.50 × 10 <sup>1</sup>	-1.78	-1.75	1.50 × 10 <sup>1</sup>	1.50 × 10 <sup>1</sup>
CaX <sub>2</sub>		0.80														
MgX <sub>2</sub>		0.60														
NaX		0.00														

<sup>a</sup> Saturation index (SI) = log [Ion activity product (IAP)]/[Equilibrium constant (KT) at temperature T]. Negative SI indicating undersaturation of the liquid with the mineral phase while positive values imply supersaturation of the liquid phase with the mineral

<sup>b</sup> Inverse modeling results using PHREEQC v.3 (Parkhurst and Appelo 1999) implemented with Minteq V. 4 thermodynamic database. Positive = mass entering water and negative = mass leaving water. Phase mole transfers indicate dissolution and precipitation, respectively

Bold value highlights the shift from saturated state to undersaturation state of the mineral phase after surface complexation reactions opposite to observed trends in other minerals

The mole transfer model further implicates that an amount of Na is realized from cation exchange as shown by the dissolution of NaX when groundwater evolves from C4 to C3. In the model (Table 5), the mole transfer for NaX shows that the greater amount of Na is due to cation exchange when compared with the mole transfers of halite and mirabilite. This concludes that the main source of Na in the alluvial aquifer of the North Rukuru–Songwe alluvial plain is due to cation exchange mostly from silicate sources. It further implies that evaporites are higher toward the discharge zone than the recharge zone which is in tandem with the fact that evapotranspiration is greater in the C3 zone than the C4 zone.

## Conclusions

The groundwater showed varying concentrations of trace elements. It is evident that CO<sub>2</sub> dissolution and organic matter degradation supplement to the carbonate mineral dissolution to elevate the HCO<sub>3</sub> levels observed in the groundwater samples studied. Hydrothermal activities in the Mpata gap can have a resultant effect on the observed isotopic values of KA-09 and KA-10 samples. This fact needs further studies. Furthermore, rainwater fall out is the source of groundwater recharge as evident by the  $\delta^{18}\text{O}$  and  $\delta^2\text{H}$  isotopic ratio, while vertical recharge and mixing are the main process as shown by the  $\delta^{18}\text{O}$  versus TDS plot. The regression analysis of NO<sub>3</sub> versus  $\delta^{18}\text{O}$  did not yield any plausible impact of irrigation return flow on groundwater stable isotope modification. It was noted that there was no significant difference between the observed *d*-excess and the *y*-intercept of the GMWL suggesting minimal impact of evaporative processes on isotopic signature of the study area.

From cluster analysis, it is evident along the North Rukuru River that areas in the west had higher TDS, As, Ba, Li, Ni, Se and Sr while the eastern part was consistent with higher values of F, Fe, Mn, Pb and Sb. Industrial and commercial activities that are prevalent in the eastern part may be responsible in part to the appreciable levels of heavy metals, while coal-related activities in the west could be responsible for the levels of trace elements. The cluster median values of stable isotopes show that groundwater in the east is more depleted than in the west due to isotope fractionation and rock–water interaction as water flows eastwards. PCA deduced associations among elements and identified underlying factors, especially pH and redox conditions that affect the observed levels. It is noted that precipitation/dissolution, pH (and Eh), residence time and aquifer thickness affect the levels of trace elements observed in the groundwater.

The geochemical modeling results confirm that indeed groundwater type in the study area is affected by dissolution of CO<sub>2</sub> with most of the carbonate minerals being undersaturated in all clusters. Surface complexation plays a key role in controlling trace element species, especially higher removal efficiencies observed for higher redox state species. Thus, the reduced form such as As(III) is retained less onto the surface complex. As(III) is more toxic than As(V), which may result in health problems in the area if unchecked. The inverse modeling shows that groundwater evolves from a predominantly Ca type to mixed cation along the North Rukuru flow path and that evaporites increase toward the discharge zone.

The outcome of this study is significant in that it provides more information on geochemical evolution and groundwater provenance in Karonga north. Besides, the assessment of groundwater quality in terms of trace elements is a very critical component that has been lacking in properly managing groundwater in this area. The study and method of assessment may prove significant to the region since the alluvial plain studied is part of the extensive Great Rift Valley System extending regionally from Tanzania running along the Lake Malawi into the Indian Ocean along the Zambezi River in Mozambique. Thus, the contribution of this study can prove useful in studies along this valley floor and extend to the entire Southern Africa region which is consistently underlain by the extensive Basement complex. Around the world, these findings and assessment method can be used as reference in studying similar alluvial aquifers.

**Acknowledgments** This study received material support from University of Malawi. Mr. A Maliro and Mr. D. Chimutu helped us in sampling and field data collection. Colleagues from the Department of Water in Karonga district assisted greatly during sampling work. This research was financially supported by the National Natural Science Foundation of China (Nos. 41521001, 41372254 and 41202168).

## References

- Aggarwal PK, Fröhlich K, Kulkarni KM, Gourcy LL (2004) Stable isotope evidence for moisture sources in the Asian summer monsoon under present and past climate regimes. *Geophys Res Lett* 31:L08203. doi:10.1029/2004GL019911
- Allison JD, Brown DS, Kevin J (1991) MINTEQA2/PRODEFA2, a geochemical assessment model for environmental systems: Version 3.0 user's manual. Environmental Research Laboratory, Office of Research and Development, US Environmental Protection Agency, Athens
- Bhattacharya S, Gupta K, Debnath S, Ghosh UC, Chattopadhyay D, Mukhopadhyay A (2012) Arsenic bioaccumulation in rice and edible plants and subsequent transmission through food chain in Bengal basin: a review of the perspectives for environmental health. *Toxicol Environ Chem* 94:429–441
- Boutaleb S, Bouchaou L, Hsissou Y, Mudry J, Mania J, Chauve P (2000) Hydrogeologic effects on the quality of water in the Oued

- Issen watershed, western Upper Atlas Mountains, Morocco. *Hydrogeol J* 8:230–238
- Breitenbach SF, Adkins JF, Meyer H, Marwan N, Kumar KK, Haug GH (2010) Strong influence of water vapor source dynamics on stable isotopes in precipitation observed in Southern Meghalaya, NE India. *Earth Planet Sci Lett* 292:212–220
- Chen K, Jiao JJ, Huang J, Huang R (2007) Multivariate statistical evaluation of trace elements in groundwater in a coastal area in Shenzhen, China. *Environ Pollut* 147:771–780. doi:10.1016/j.envpol.2006.09.002
- Chilton PJ, Smith-Carington AK (1984) Characteristics of the weathered basement aquifer in Malawi in relation to rural water supplies. In: Walling DE, Foster SSD, Wurzel P (eds) Proceedings of the Harare Symposium. IAHS Publ no.144, Harare. pp 57–72
- Cloutier V, Lefebvre R, Therrien R, Savard MM (2008) Multivariate statistical analysis of geochemical data as indicative of the hydrogeochemical evolution of groundwater in a sedimentary rock aquifer system. *J Hydrol* 353:294–313. doi:10.1016/j.jhydrol.2008.02.015
- Craig H (1961) Isotopic variations in meteoric waters. *Science* 133:1702–1703
- Dill H, Ludwig R-R, Kathewera A, Mwenelupembe J (2005) A lithofacies terrain model for the Blantyre Region: implications for the interpretation of palaeosavanna depositional systems and for environmental geology and economic geology in southern Malawi. *J Afr Earth Sci* 41:341–393
- Dulanya Z, Morales-Simfors N, Sivertun Å (2010) Comparative study of the silica and cation geothermometry of the Malawi hot springs: potential alternative energy source. *J Afr Earth Sc* 57:321–327. doi:10.1016/j.jafrearsci.2009.11.001
- Fagereng Å (2013) Fault segmentation, deep rift earthquakes and crustal rheology: insights from the 2009 Karonga sequence and seismicity in the Rukwa–Malawi rift zone. *Tectonophysics* 601:216–225. doi:10.1016/j.tecto.2013.05.012
- Fass T, Cook PG, Stieglitz T, Herczeg AL (2007) Development of saline ground water through transpiration of sea water. *Ground Water* 45:703–710. doi:10.1111/j.1745-6584.2007.00344.x
- Fontes JC, Saliege JF, Zuppi GM, Pouchon P (1980) Environmental isotope study of groundwater systems in the Republic of Djibouti. *Arid-zone Hydrology. Investigations with Isotope Techniques: proceedings of an advisory group meeting on application of isotope techniques in arid zones hydrology*, pp 237–262
- Gat J, Tzur Y (1968) Modification of the isotopic composition of rainwater by processes which occur before groundwater recharge. Weizmann Institute of Science, Rehovoth
- Ghabayen SMS, McKee M, Kemblowski M (2006) Ionic and isotopic ratios for identification of salinity sources and missing data in the Gaza aquifer. *J Hydrol* 318:360–373. doi:10.1016/j.jhydrol.2005.06.041
- Horst A, Mahlknecht J, Merkel BJ (2007) Estimating groundwater mixing and origin in an overexploited aquifer in Guanajuato, Mexico, using stable isotopes (strontium-87, carbon-13, deuterium and oxygen-18). *Isot Environ Health Stud* 43:323–338
- Levins I, Gosk E (2008) Trace elements in groundwater as indicators of anthropogenic impact. *Environ Geol* 55:285–290
- Macheyeki AS, Mdala H, Chapola LS, Manhiça VJ, Chisambi J, Feitio P, Ayele A, Barongo J, Ferdinand RW, Ogubazghi G, Goitom B, Hlatywayo JD, Kianji GK, Marobhe I, Mulowezi A, Mutamina D, Mwano JM, Shumba B, Tumwikirize I (2015) Active fault mapping in Karonga–Malawi after the December 19, 2009 Ms 6.2 seismic event. *J Afr Earth Sc* 102:233–246. doi:10.1016/j.jafrearsci.2014.10.010
- Mapoma HWT, Xie X (2014) Basement and alluvial aquifers of Malawi: an overview of groundwater quality and policies. *Afr J Environ Sci Technol* 8:190–202. doi:10.5897/ajest2013.1639
- Mapoma HWT, Xie X, Zhang L (2014) Redox control on trace element geochemistry and provenance of groundwater in fractured basement of Blantyre, Malawi. *J Afr Earth Sci* 100:335–345. doi:10.1016/j.jafrearsci.2014.07.010
- Mapoma HWT, Xie X, Pi K, Liu Y, Zhu Y (2016) Understanding arsenic mobilization using reactive transport modeling of groundwater hydrochemistry in the Datong basin study plot, China. *Environ Sci Process Impacts* 18:371–385. doi:10.1039/C5EM00621J
- Marfia A, Krishnamurthy R, Atekwana EA, Panton W (2004) Isotopic and geochemical evolution of ground and surface waters in a karst dominated geological setting: a case study from Belize, Central America. *Appl Geochem* 19:937–946
- Merkel BJ, Planer-Friedrich B (2005) *Groundwater geochemistry: a Practical Guide to Modeling of Natural and Contaminated Aquatic Systems*. Springer, Berlin
- Mkandawire PP (2004) Groundwater resources of Malawi. In: Appelgren B (ed), *Managing Shared Aquifer Resources in Africa*. UNESCO, France. pp 91–94
- Monjerezi M, Vogt RD, Aagaard P, Gebu AG, Saka JD (2011) Using 87 Sr/86 Sr,  $\delta^{18}\text{O}$  and  $\delta^2\text{H}$  isotopes along with major chemical composition to assess groundwater salinization in lower Shire valley, Malawi. *Appl Geochem* 26:2201–2214
- Parkhurst DL, Appelo CAJ (1999) *User's guide to PHREEQC (Version 2): a computer program for speciation, batch-reaction, one-dimensional transport, and inverse geochemical calculations*. Water-Resources Investigations Report 99–4259. US Geological Survey, Denver, p 326
- Praamsma T, Novakowski K, Kyser K, Hall K (2009) Using stable isotopes and hydraulic head data to investigate groundwater recharge and discharge in a fractured rock aquifer. *J Hydrol* 366:35–45
- Salbu B, Steinnes E (1995) *Trace elements in natural waters*. CRC Press, Boca Raton
- Smedley P, Kinniburgh D (2002) A review of the source, behaviour and distribution of arsenic in natural waters. *Appl Geochem* 17:517–568. doi:10.1016/S0883-2927(02)00018-5
- Subyani AM (2004) Use of chloride-mass balance and environmental isotopes for evaluation of groundwater recharge in the alluvial aquifer, Wadi Tharad, western Saudi Arabia. *Environ Geol* 46:741–749
- Sukhija B, Reddy D, Nagabhushanam P, Bhattacharya S, Jani R, Kumar D (2006) Characterisation of recharge processes and groundwater flow mechanisms in weathered-fractured granites of Hyderabad (India) using isotopes. *Hydrogeol J* 14:663–674
- Talabi AO (2013) Hydrogeochemistry and stable isotopes ( $\delta^{18}\text{O}$  and  $\delta^2\text{H}$ ) assessment of Ikogosi spring waters. *Am J Water Res* 1:25–33
- Turner J, Arad A, Johnston C (1987) Environmental isotope hydrology of salinized experimental catchments. *J Hydrol* 94:89–107
- USGS (2004) Resources on isotopes. [http://wwwrcamnl.wr.usgs.gov/isoig/period/h\\_iig.html](http://wwwrcamnl.wr.usgs.gov/isoig/period/h_iig.html). Accessed 1 Oct 2015
- Valipour M (2014a) Drainage, waterlogging, and salinity. *Arch Agron Soil Sci* 60:1625–1640. doi:10.1080/03650340.2014.905676
- Valipour M (2014b) Future of the area equipped for irrigation. *Arch Agron Soil Sci* 60:1641–1660. doi:10.1080/03650340.2014.905675
- Valipour M (2015a) A comprehensive study on irrigation management in Asia and Oceania. *Arch Agron Soil Sci* 61:1247–1271. doi:10.1080/03650340.2014.986471

- Valipour M (2015b) Future of agricultural water management in Africa. *Arch Agron Soil Sci* 61:907–927. doi:[10.1080/03650340.2014.961433](https://doi.org/10.1080/03650340.2014.961433)
- Valipour M (2015c) What is the tendency to cultivate plants for designing cropping intensity in irrigated area? *Adv Water Sci Technol* 2:01–12
- Valipour M, Ziatabar Ahmadi M, Raeini-Sarjaz M, Gholami Sefidkouhi MA, Shahnazari A, Fazlola R, Darzi-Naftchali A (2015) Agricultural water management in the world during past half century. *Arch Agron Soil Sci* 61:657–678. doi:[10.1080/03650340.2014.944903](https://doi.org/10.1080/03650340.2014.944903)
- Wanda E, Monjerezi M, Mwatseteza JF, Kazembe LN (2011) Hydro-geochemical appraisal of groundwater quality from weathered basement aquifers in Northern Malawi. *Phys Chem Earth Parts A/B/C* 36:1197–1207
- Wanda EMM, Gulula LC, Phiri A (2013) Hydrochemical assessment of groundwater used for irrigation in Rumphu and Karonga districts, Northern Malawi. *Phys Chem Earth Parts A/B/C* 66:51–59. doi:[10.1016/j.pce.2013.09.001](https://doi.org/10.1016/j.pce.2013.09.001)
- WHO (2011) Guidelines for drinking-water quality, 4th edn. World Health Organization, Geneva
- Wright DK, Thompson J, Mackay A, Welling M, Forman SL, Price G, J-x Zhao, Cohen AS, Malijani O, Gomani-Chindebvu E (2014) Renewed geoarchaeological investigations of Mwanganda's Village (Elephant Butchery Site), Karonga, Malawi. *Geoarchaeology* 29:98–120. doi:[10.1002/geo.21469](https://doi.org/10.1002/geo.21469)